BUCKLING OF CHANNEL FLANGES DURING BENDING IN THE WEAK DIRECTION

by

RICHARD C. HASKELL

BE-CE University of Southern California

SUBMITTED IN PARTIAL FULFILLMENT OF THE
REQUIREMENTS FOR THE DEGREE OF
MASTER OF SCIENCE

at the

MASSACHUSETTS INSTITUTE OF TECHNOLOGY

August 1960

Signature of Author.......................................
Department of Civil and Sanitary
Engineering, August 22, 1960

Certified by... ....
Thesis Supervisor

Accepted by.....................................
Chairman, Departmental Committee on
Graduate Students

ACKNOWLEDGEMENTS

The author would like to express his sincere thanks to Professor J. M. Biggs, whose guidance and patient advice made this thesis possible. Appreciation is also extended to Don Gunn for his preparation of test specimens and Saul Nuccitelli for his advice on strain gage techniques.

ABSTRACT

BUCKLING OF CHANNEL FLANGES DURING BENDING IN THE WEAK DIRECTION

by

RICHARD C. HASKELL

Submitted to the Department of Civil and Sanitary Engineering on August 22, 1960 in partial fulfillment of the requirements for the degree of Master of Science.

The problem of channel flange crippling during bending about an axis parallel to the web had been given very little treatment since it did not occur too often in practice. One rigorous analysis and three approximate analyses of determining critical flange stresses were discussed, and experiments were performed to spot check these theories.

A method of determining the ultimate failure moment for channels was investigated from a semi-empirical approach.

Thesis Supervisor: J. M. Biggs

Title: Associate Professor of Structural Engineering

TABLE OF CONTENTS

List of Figures

Summary

The object of this thesis was to spot check various theoretical methods of determining critical buckling stresses, and to formulate an approach to finding the ultimate moment a channel can resist when loaded in bending in the weak direction.

Four theoretical buckling analyses were discussed, and tests were run on three different channel sections. Critical buckling moments and ultimate moments were determined by observation of specimens and analysis of strain gage data.

Of the four methods shown in figure 39, it was found that method (a) was the best method of predicting critical buckling stresses for materials with proportional limit below 18.0 ksi. For material with a higher proportional limit method (b) was used to be conservative. Methods (c) and (d) indicated large errors on the conservative side, especially at the low buckling stresses.

A semi-empirical method of predicting ultimate strength was discussed, and formulas were developed. However, the results were inconclusive and more test data was required to substantiate the theory. A conservative formula for predicting ultimate strength was

$$M_{ult} = .67\ \sigma_{cr} b_f^2 t \qquad (19a)$$

1.0 Previous Work

A search of the literature showed that very little work had been done on this subject. The people most interested in formed sheet metal sections were in the air frame industry and these people were usually concerned with minimum weight design. For this reason it was found that a channel section in bending about an axis parallel to the web was rarely employed in practice.

There were two theoretical approaches to finding the critical buckling stress of these channel flanges which had been presented to date. The first approach was derived by Bell Aircraft Corporation in an unpublished report with the aid of references 2, 3, and 4. The results of this report were shown in a graph in reference 1.

Another study which is analogous to the problem was done by Bijlaard and presented in reference 5. Bijlaard derived formulas for critical compressive stresses of hinged and fixed flanges under a linearly varying stress. The critical stress for a partially restrained channel flange was somewhere in between the cases of pinned and fixed flanges. Since the available methods of arriving at the amount of restraint were approximate the Bijlaard theory did not seem as accurate as the graph used by Bell Aircraft.

Another approach to flange buckling problems which was often used by aircraft designers was based on ultimate strength theory. A semi-empirical method that gives good results for uniformly loaded flanges was given in reference 9. However, for the case under consideration another ultimate strength approach was developed.

There was no previously available test data on either critical buckling stress or ultimate strength which could be found.

2.0 Theoretical Approaches

A firm understanding of plate buckling theory was necessary to analyze this problem correctly. The basic formula to determine the critical crippling stress in plates or plate elements with various compressive stresses was

$$\sigma_{cr} = \frac{k\pi^2 \sqrt{\tau}\, E}{12(1 - \nu^2)} \left(\frac{t}{b}\right)^2 \qquad (1)$$

where:

ν = Poisson's ratio

σ_{cr} = critical compressive crippling stress - ksi

t = plate thickness - inches

b = plate width - inches

$\sqrt{\tau}$ = plasticity coefficient used in reference 2 for stresses in the inelastic range

τ = E_t/E where E_t = tangent modulus, the slope of the stress-strain curve at any particular point.

k = constant which is dependent on the restraint of the plate along its unloaded edges and the distribution of the stress across the width of the plate.

The basic differential equation for instability of plates in the elastic range was

$$\frac{Et^3}{12(1-\nu^2)}\left(\frac{\partial^4 w}{\partial x^4} + 2\frac{\partial^4 w}{\partial x^2 \partial y^2} + \frac{\partial^4 w}{\partial y^4}\right) + \sigma_x t \frac{\partial^2 w}{\partial x^2} = 0 \quad (2)$$

where :

σ_x = stress in the direction of loading

w = plate displacement perpendicular to the plane of the plate

For the case of stress in the inelastic range, equation (2) was modified. Different authors gave different modifications. Probably the most widely accepted plasticity hypothesis was derived by Stowell in reference 8, but the results were far too complicated to be used in design. A more simple approach was given by Bleich in reference 2, and was sufficiently accurate for practical purposes.

When the buckling stress exceeded the proportional limit of the material, Young's modulus, E, no longer held. Bleich assumed that when σ_x exceeded proportional limit, the tangent modulus, E_t was effective in the direction of loading and Young's modulus, E, was effective in the direction perpendicular to loading. In equation (2) the three terms in parenthesis were noted. The first term corresponded to bending of strips parallel to the x axis. These strips were stressed by the longitudinal force, $\sigma_x t$. This term was then modified to read $\frac{\partial^4 w}{\partial x^4}(\tau)$. In the same manner the third term corresponded to strips in bending perpendicular to the x axis which were free of externally applied stresses. Therefore this term remained unchanged. The middle term in parenthesis was associated with the distortion of a square plate due to twising moments on the element. This term was effected by plastic action in a complicated way, and was multiplied by a coefficient having a value somewhere between 1 and τ. The value $\sqrt{\tau}$ was used somewhat arbitrarily. Thus equation (2) became

$$\frac{Et^3}{12(1-\nu^2)}\left(\tau\frac{\partial^4 w}{\partial x^4} + 2\sqrt{\tau}\frac{\partial^4 w}{\partial x^2\,\partial y^2} + \frac{\partial^4 w}{\partial y^4}\right) + \sigma_x t\frac{\partial^2 w}{\partial x^2} = 0 \tag{2a}$$

Poisson's ratio, ν, was effected slightly in the inelastic range, but since the effect of ν on equation (2a) was small, the change due to inelastic behavior was ignored.

Solution of equation (2a) resulted in the algebraic plate crippling equation, (1). It was known that the plasticity coefficient lay somewhere between E_s/E and E_t/E where E_s was the secant modulus. Bleich's value of $\sqrt{E_t/E}$ was a conservative value and was considered as a lower limit for most cases. Bleich defined τ as follows:

$$\tau \doteq E_t/E = \frac{(\sigma_y - \sigma_{cr})\ \sigma_{cr}}{(\sigma_y - \sigma_p)\ \sigma_p} \tag{3}$$

σ_y = material yield stress - ksi

σ_p = material proportional limit - ksi

It was noted that since γ was dependent upon σ_{cr}, a trial and error solution of (1) was necessary. This was avoided by algebraic manipulation of (1) to read

$$\sigma_{cr}/\sqrt{\gamma} = \frac{k\,\pi^2 E}{12(1-\nu^2)}\left(\frac{t}{b}\right)^2 \qquad (1a)$$

Tables were available to determine σ_{cr} from corresponding values of $\sigma_{cr}/\sqrt{\gamma}$ for various materials.

For the case of a sheet metal channel in bending in the weak direction the only unknown in (1) was the constant, k. Four different methods of determining k were considered, and were presented in figure 39, as a function of (web depth/flange width). These methods were summarized as follows: (a) An infinitely long hinged flange under uniformly distributed stress was assumed. (b) An infinitely long partially restrained flange under uniform stress was assumed. (c) (Bijlaard's analysis) The flange was assumed infinitely long and under a linearly varying stress. A coefficient of restraint proportional to the coefficient for a uniformly distributed stress was used. (d) (Bell Aircraft graph) The actual case of a channel loaded in bending in the weak direction was assumed.

This paper was only concerned with the most common case where the web thickness equaled the flange thickness and the unsupported flange length was great compared to the flange width.

2.1 Method (a): Assuming an Infinitely Long Uniformly Stressed Hinged Flange

Solution of equation (2a) using the boundary conditions of method (a) for an infinitely long hinged flange under uniform stress led to the basic algebraic equation (1) for crippling of plates. In this case the value for k was .425 as shown by the straight line in figure 39. This well known solution was presented by Timoshenko in reference 7.

2.2 Method (b): Assuming an Infinitely Long Uniformly Stressed Partially Restrained Flange

The case of method (b) for a restrained flange was solved by Bleich in reference 2. Bleich introduced the concept of the coefficient of restraint, ζ, to determine the value of k. The coefficient of restraint expressed the amount of fixity provided to a plate element, by the adjoining plate elements. It depended upon the cross section dimensions and the stress distribution. For the case of a channel under uniform compressive stress, the coefficient of restraint for the flanges was

$$\zeta = \frac{t_f^3}{t_w^3} \; \frac{b_w}{b_f} \; \frac{1}{1 - .106\,(t_f/t_w)^2 (b_w/b_f)^2} \qquad (4)$$

where:

t_f = flange thickness - inches

t_w = web thickness - inches

b_f = flange width - inches

b_w = web width - inches

This equation was valid for $9.4\ (t_w/t_f)^2(b_f/b_w)^2 \geq 1.0$. When the above value was less than 1.0 the web plate crippled at a lower load than the flange, so the flanges then provided restraint for the web.

To determine the value of k the following equation was used:

$$k_r = \left(\frac{2}{3\rho+4} + .65\right)^2 \qquad (5)$$

where:

k_r = k for the restrained case under uniform load.

For the case being considered where $t_f = t_w$, k_r was found as a function of b_w/b_f in Figure 41 and plotted in Figure 39.

2.3 Method (c): Bijlaard's Theory Assuming a Uniform Stress Coefficient of Restraint.

Method (c) of finding σ_{cr} of a channel was taken from Bijlaard's paper, reference 5. Bijlaard analyzed hinged and fixed flanges of infinite length subjected to a stress that varied linearly with flange width. An energy approach was used and the equations were solved by a method of finite differences. The flange was assumed to buckle in the shape of a sine curve in the longitudinal direction for both the fixed and pinned cases. In the lateral direction, for the fixed case the deflection was expressed in terms of the normal mode of vibration of a cantilever beam. For the hinged case the flange deflection was assumed to increase linearly with the distance from the hinge. For application to the case under consideration, two modifications were made.

To arrive at a plasticity factor, η, Bijlaard published graphs that expressed a plasticity constant in terms of E_s/E at the edge of highest strain. This constant was then plugged into an equation to determine η, and this factor, η, was in turn used in equation (1) in place of $\sqrt{\tau}$ to find σcr. The advantage of Bijlaard's plasticity factor was that the graphs were applicable to all materials, but values of E_s/E were not readily available for various materials. Also the method involved a trial and error solution because η was dependent on σcr. Since values of E_s/E vs. stress for mild steel sheet could not be easily plotted, and since Bijlaard's method involved a great deal of arithmetic, it was decided to use Bleich's plasticity coefficient, $\sqrt{\tau}$, in place of η. The error involved was slight.

The second modification to Bijlaard's theory was the determination of a proper coefficient of restraint. The procedure was to find values of k for Bijlaard's hinged and fixed cases, and then determine an intermediate value proportional to the intermediate value for the case of a uniformly stressed channel given in reference 2. This gave results which were generally conservative as expected, since a web in tension during bending supplied more restraint than a web in compression during axial loading.

Values of k vs. b_w/b_f were plotted in figure 39 and compared to values obtained by methods (a), (b), and (d). These values were determined by the following algebraic manipulation of Bijlaard's equations, and appeared in figure 41.

In reference 1, k for the fixed and pinned cases was expressed as a function of α, where α is an expression for the linear stress distribution as shown in Figure 42.

$$\alpha = 1 - \frac{\sigma_h}{\sigma_f} \text{ (compressive stress = +)} \qquad (6)$$

where:

σ_h = stress at hinged or restrained edge - ksi

σ_f = stress at free edge - ksi

To express α in terms of b_w/b_f, it was necessary to locate the elastic neutral axis, $\bar{y}$, of the channel. From figure 43,

$$\bar{y} = \frac{\Sigma A_y}{\Sigma A} \quad \frac{b_f(b_f/2) + (b_w/2)b_f}{b_f + b_w/2} \times \left(\frac{b_f}{b_f}\right) = \frac{(b_f + b_w)}{2 + b_w/b_f}$$

$$\frac{\sigma_h}{\sigma_f} = \frac{-(b_f - \bar{y})}{\bar{y}} = \frac{-[b_f - \frac{b_f + b_w}{2 + b_w/b_f}]}{\frac{b_f + b_w}{2 + b_w/b_f}} \times (\frac{2 + b_w/b_f}{2 + b_w/b_f}$$

$$= - \frac{b_f}{b_f + b_w}$$

$$\alpha = 1 - \frac{\sigma_h}{\sigma_f} = 1 + \frac{b_f}{b_f + b_w} = \frac{2b_f + b_w}{b_f + b_w}$$

$$\boxed{\alpha = \frac{2 + b_w/b_f}{1 + b_w/b_f}} \qquad (6a)$$

It was then possible to solve for α knowing b_w/b_f. In reference 5, the value of $(k_B)_h$ for hinged flanges was

$$(k_B)_h = \frac{16.8}{\pi^2 (4 - \alpha)} \qquad (8)$$

where:

$(k_B)_h$ was Bijlaard's constant, k, for hinged flanges.

For fixed flanges $(k_B)_f$ vs. α is plotted in figure 9 of reference 5, where $(k_B)_f$ was Bijlaard's constant, k, for fixed flanges.

Using equations (4) and (5) values of k_r were determined for restrained channel flanges when the channel was under uniform stress. The proportioned k value for moment loading was found by the following equation:

$$k = \frac{k_r - k_f}{k_f - k_h} \quad (k_B)_f - (k_B)_h \qquad + (k_B)_h \tag{9}$$

where:

k_r = k for uniformly loaded restrained flange

k_h = k for uniformly loaded hinged flange = .425

k_f = k for uniformly loaded fixed flange = 1.277

$(k_B)_h$ = k for Bijlaard's hinged flange under linear stress distribution (reference 5)

$(k_B)_f$ = k for Bijlaard's fixed flange under linear stress distribution (reference 5)

2.4 Method (d): Bell Aircraft Solution of Channel in Bending about Axis Parallel to the Web

Method (d) of determining the plate buckling factor, k, was a method derived by Bell Aircraft Corporation in an unpublished report with the aid of references 2, 3, and 4. The results appeared in a graph in reference 1 which was reproduced in Figure 39. An energy approach was used in conjunction with an application of the moment distribution method explained in reference 4. Figure 44 was considered.

The stability condition was

$$T = V_1 \text{ and } V_2 \tag{10}$$

where:

T = work done by external compressive forces

V_1 = strain energy in the plate

V_2 = strain energy in the elastic restraining medium

$$T = \frac{1}{2} \int_0^b \int_{-\lambda/2}^{\lambda/2} t\sigma_x \left(\frac{\partial w}{\partial x}\right)^2 dx\, dy \qquad (11)$$

$$V_1 = \frac{E t^3}{2 \times 12(1-\nu^2)} \int_0^b \int_{-\lambda/2}^{\lambda/2} \left\{ \left(\frac{\partial^2 w}{\partial x^2} + \frac{\partial^2 w}{\partial y^2}\right)^2 + 2(1-\nu) \left[\left(\frac{\partial^2 w}{\partial x \partial y}\right)^2 - \left(\frac{\partial^2 w}{\partial x^2} \frac{\partial^2 w}{\partial y^2}\right) \right] \right\} dx\, dy \qquad (12)$$

$$V_2 = \frac{4S_o}{2} \int_{-\lambda/2}^{\lambda/2} \left[\left(\frac{\partial w}{\partial y}\right)_{y=o} \right]^2 dx \qquad (13)$$

S_o = stiffness per unit length of elastic medium or moment for 1/4 radian rotation

The proper boundary conditions from Figure 44 were

$$(w)_{y=o} = 0 \qquad (14a)$$

$$\frac{Et^3}{12(1-\nu^2)} \left(\frac{\partial^2 w}{\partial y^2} + \nu \frac{\partial^2 w}{\partial x^2}\right)_{y=0} = 4S_o \left(\frac{\partial w}{\partial y}\right)_{y=0} \qquad (14b)$$

$$\frac{Et^3}{12(1-\nu^2)} \left(\frac{\partial^2 w}{\partial y^2} + \nu \frac{\partial^2 w}{\partial x^2}\right)_{y=b} = 0 \qquad (14c)$$

$$\frac{Et^3}{12(1-\nu^2)} \frac{\partial^3 w}{\partial y^3} + (2-\nu)\left(\frac{\partial^3 w}{\partial x^2 \partial y}\right)_{y=b} = 0 \qquad (14d)$$

where (14b) and (14c) expressed the moment condition at points y=0 and y=b respectively, and (14d) expressed the shear condition at y=b.

The assumed deflection was

$$w = \left\{ A\,\frac{y}{b} + B\left[\left(\frac{y}{b}\right)^5 + a_1\left(\frac{y}{b}\right)^4 + a_2\left(\frac{y}{b}\right)^3 + a_3\left(\frac{y}{b}\right)^2\right]\right\}\cos\frac{\pi x}{\lambda} \quad (15)$$

where A and B were arbitrary deflection amplitudes. When A = 0 the edge was clamped, and when B = 0 the edge was pinned. The assumed deflection in equation (15) was a sine curve in the direction of length, and the sum of a straight line rotation deflection and cantilever beam deflection in the direction of the width.

Method (d) above was a rigorous solution of the problem of a channel in bending in the weak direction. Methods (a), (b), and (c), demonstrated conservative approximations which might be used by designers if more accurate data were not available.

2.5 Ultimate Strength Considerations

Determining ultimate strength of compression flanges was a very complicated mathematical problem, and empirical or semi-empirical methods were usually used. Gerard in reference 9 had developed a method that seemed to work for plates and flanges under uniform load. His method assumed that after tha flange buckled at the free edge, the member continued to take load until the yield point was reached at the flange-web connection. In the present case this theory did not hold up, since the connection area between flange and web carried small stresses at ultimate load.

A theory of predicting ultimate moment was discussed in paragraph 5.2 of this thesis. It assumed a particular stress distribution at failure, which varied with cross section dimensions. The method was semi-empirical in nature, and much more test data was necessary before it could be considered accurate.

3.0 Procedure

3.1 Method of Attack

The purpose of these tests was to spot check the theoretical methods of determining critical buckling stresses, and to formulate an approach of finding the ultimate moment a channel could resist when loaded in the weak direction.

The first step in testing was to determine the material to be used and its properties. Cold rolled annealed mild steel strip was selected because of its thickness tolerances (±.002"), its freedom from residual stresses, and its linear stress-strain curve. Tensile tests were run on specimens cut from the same strip as the channel sections, and stress-strain diagrams were plotted. From the stress-strain diagrams average values of proportional limit, yield point, and Young's modulus were found.

Using the Bell Aircraft curve in figure 39, three channel test sections were designed and constructed.

The material used was the same thickness throughout, and the width of web was held constant. The flange width was varied on the three sections to give critical crippling stresses (1) below the proportional limit, (2) at the porportional limit, and (3) in the inelastic range. The channels were all the same length and were all loaded in pure bending at the same loading and support points. Sheared edges were ground off to eliminate strain hardening.

The 20 inch span between load application was ground down to assure the highest stresses occurred in this area and not at the point of load application where shear stresses were present. Care was taken to avoid any pounding or straightening which might work harden the material in critical areas.

A mathematical check was made of channel #3 to determine if the channel would fail by lateral buckling below the ultimate load. It was found that lateral buckling was not critical.

Strain gages were located on the channel at midspan to determine the stress distribution at various applied moments. Gages were located as shown in figures 28, 30, and 32. The double gages were placed on both sides of one flange and connected in series to eliminate any effects from the flange bending out of its plane. Since no eccentric load occurred in the web single gages were adequate there. The single gage on the opposite flange was to indicate if the channel was loading concentrically. The double gage nearest the web was located at the elastic neutral axis to note at what moment the neutral axis started shifting.

3.2 Description of Apparatus

Photographs of the tensile testing and channel testing apparatus were shown in figures 1 through 6. A sketch of the channel testing apparatus was shown in figure 7, and sketches of tensile specimens and channel sections were shown in figures 8 and 9.

3.3 Description of Procedure

3.3.1 Tests to Determine Material Properties

Tensile specimens were made from the strip used to form the channel sections. These specimens conformed to the standard ASTM specifications for tensile testing sheet metal as described in reference 10 and figure 8.

The specimens were measured with micrometers and tested in a 5,000 lb. capacity Baldwin tensile testing machine, using a Metzger extensometer with a 2 inch grip reading to .0001". Incremental load and deflection readings were taken as shown in figures 15, 16, and 17.

3.3.2 Tests of Channel Sections

Three sheet metal channel sections were formed as shown in figure 9. Baldwin A-7 120 ohm, 1.96 gage factor strain gages were attached as shown in figures 28, 30, and 32. Double gages were connected in series. The resistance changes were read with a Baldwin SR-4 strain indicator which read strain directly to the nearest 0.1 microinch. The channel sections were measured using micrometers and placed in a 10,000 lb. capacity hand operated beam testing machine as shown in figure 7. Loads were applied incrementally as shown in figures 25, 26, and 27. The loading machine was accurate to the nearest two pounds and strain gage readings were recorded at each incremental load.

On channel #1 loads were increased on up to failure, but on channels #2 and #3 the load was applied, released and reapplied alternately. The loads causing crippling in the extreme fibres and ultimate failure were noted.

3.4 Methods of Making Computations and of Plotting Curves

3.4.1 Determining Material Properties

The data from the tensile specimens was reduced in the usual manner and plotted as stress vs. strain in figures 18 through 24. The yield point was determined by the .2% offset method as shown on the graphs. The E value was taken as the initial straight slope of the curve. The porportional limit, which was difficult to obtain consistantly, was taken as the stress at that point of the curve which first deviated from a straight line. Due to initial unrecorded stresses which were unavoidable, each curve had a small offset stress from the zero point which was compensated for in the calculations. Material properties for each specimen were calculated on the stress-strain curve, and the sum was averaged to determine the yield point, proportional limit, and Young's modulus of the material Ultimate strengths were recorded.

3.4.2 Plotting Values of k vs. b_w/b_f

Four curves of k vs. b_w/b_f were computed in figures 39 and plotted in accordance with methods (a), (b), (c), and (d) of paragraph 2.0. The computations for these plots were as follows.

Method (a) k $\neq$ .425 (straight line)

Method (b) k from equation (5) (see figure 41)

Method (c) k from equation (9) (see figure 41)

Method (d) k from reference 1.

3.4.3 Design of Channel Sections

Channel sections were designed using equation (1) and the Bell Aircraft curve reproduced in figure 39. Material properties as found in paragraph 3.4.1 were used in the calculations. For each channel the following dimensions were constant:

Web thickness = flange thickness = .0625"

Web depth = 4.00" (outside dimension)

Channel span = 40.0"

Distance between load points = 20.0"

Bend radius = .062"

The flange widths were varied to give crippling stresses (1) in the elastic range, (2) at the proportional limit, and (3) in the inelastic range.

Channel #1: Assume flange width = 4.00" (outside dimension)

$$\sigma_{cr}/\sqrt{\tau} = \frac{k\pi^2 E}{12(1-\nu^2)}\left(\frac{t_f}{b_f}\right)^2 \qquad (1)$$

t_f = .0625"

b_f = 4.00 - .06/2 = 3.97"

b_w = 4.00 - .06 = 3.94"

ν = .30

E = 28.6 x 10^3 ksi

P.L. = 17.7 ksi

From figure 39, method (d):

b_w/b_f = 3.94/3.97 = .994 $\therefore$ k = 1.30

$$\sigma_{cr}/\sqrt{\tau} = \frac{1.30\pi^2 \times 28.6 \times 10^3}{12(1-.30^2)}\left(\frac{.0625}{3.97}\right)^2 = 8.35^{ksi} < 17.7$$

$$\boxed{\sigma_{cr} = 8.35 \text{ ksi}}$$

Channel #2: Assume flange width = 2.50" (outside dimension)

$$b_w/b_f = \frac{4.00 - .06}{2.50 - .03} = 1.60 \quad \therefore k = 1.15$$

$$\sigma_{cr}/\sqrt{\tau} = \frac{1.15\pi^2 \times 28.6 \times 10^3}{12(1-.30^2)}\left(\frac{.0625}{2.47}\right)^2 = 19.0 \text{ ksi} \approx 17.7$$

$$\therefore \boxed{\sigma_{cr} \approx 18.0 \text{ ksi}}$$

Channel #3: Assume flange width = 1.00" (outside dimension)

$$b_w/b_f = \frac{4.00 - .06}{1.00 - .03} = 4.10 \qquad \therefore\ k = .906$$

$$\sigma_{cr}/\sqrt{\tau} = \frac{.906\pi^2 \times 28.6 \times 10^3}{12(1 - .30^2)} \left(\frac{.0625}{.97}\right)^2 = 97.1 \text{ ksi} > 17.7$$

$\therefore\ \boxed{\sigma_{cr} \approx 29.0 \text{ ksi}}$ (slightly less than yield point)

3.4.4 Calculation of Section Properties Using Actual Channel Dimensions

The following section properties of each channel were calculated using the measured dimensions of each section and material properties found in paragraph 3.4.1. When the two flange dimensions varied the least of the two was used. Refer to figure 14.

$\bar{y}$ = neutral axis location - inches

S = section modulus - in.^{3}

I = moment of inertia - in.^{4}

3.4.5 Predicted Buckling Stresses Using Actual Dimensions

The extreme fibre buckling stresses were calculated using the actual measured cross-section dimensions. When the two flange dimensions varied, the least of the two was used.

Method (a)

Channel #1: 4.00 x 4.01 x .0610

$\tau = 1.0$

$$\sigma_{cr} = \frac{k\pi^2\sqrt{\tau}\,E}{12\,(1-\nu^2)}\left(\frac{t_f}{b_f}\right) = \frac{k\pi^2(1) \times 28.6 \times 10^3}{12\,(1-.30^2)}\left(\frac{t_f}{b_f}\right)^2$$

$$= 25.9 \times 10^3 k \left(\frac{t_f}{b_f}\right)^2$$

$b_w/b_f = 3.94/3.98 = .990, \therefore\ k = 1.300$

$$\sigma_{cr} = 25.9 \times 10^3 \times 1.300\left(\frac{.0610}{3.98}\right)^2 = \boxed{7.91\text{ ksi}}$$

Channel #2: 4.00 x 2.49 x .0618

$b_w/b_f = 3.94/2.46 = 1.60 \qquad k = 1.152$

$$\sigma_{cr}/\sqrt{\tau} = 25.9 \times 1.152\left(\frac{.0618}{2.46}\right)^2 = \underline{18.8\text{ ksi}} > 17.7$$

$$\sqrt{\tau} = \sqrt{\frac{(\sigma_y - \sigma_{cr})\sigma_{cr}}{(\sigma_y - \sigma_p)\sigma_p}} = \sqrt{\frac{(30.0 - \sigma_{cr})\,\sigma_{cr}}{(30.0 - 17.7)\quad 17.7}} = \sqrt{\frac{30.0\sigma_{cr} - \sigma_{cr}^2}{218}}$$

Solve by trial and error

1	2	3	4	5	6	7
σ_{cr}	σ_{cr}^2	$30\sigma_{cr}$	3 - 2	τ 4/218	$\sqrt{\tau}$	$\sqrt{\tau}(\sigma_{cr}/\sqrt{\tau})$
18.3	335	549	214	.982	.991	18.6
18.5	342	555	213	.978	.988	18.6

$$\boxed{\sigma_{cr} = 18.5 \text{ ksi}}$$

Channel #3: 3.99 x 1.00 x .0628

$$b_w/b_f = \frac{3.93}{.97} = 4.05 \qquad \therefore k = .910$$

$$\sigma_{cr}/\sqrt{\tau} = 25.9 \times 10^3 \left(\frac{.0628}{.97}\right)^2 = \underline{98.6 \text{ ksi}} > 17.7$$

1	2	3	4	5	6	7
σ_{cr}	σ_{cr}^2	$30\sigma_{cr}$	3 - 2	τ 4/218	$\sqrt{\tau}$	$\sqrt{\tau}(\sigma_{cr}/\sqrt{\tau})$
29.5	870	885	15	.0689	.263	26.0
29.3	859	880	21	.0964	.310	30.5

$$\boxed{\sigma_{cr} = 29.4 \text{ ksi}}$$

In a similar manner σ_{cr} was solved using methods (b), (c), and (d). The results were summarized below in figure 10.

Method	Channel	k	$\sigma_{cr}/\sqrt{\tau}$ ksi	σ_{cr} (ksi)
(a)	(1)	1.300	7.91	7.91
	(2)	1.152	18.8	18.5
	(3)	0.910	98.6	29.4
(b)	(1)	1.260	7.65	7.65
	(2)	1.026	16.7	16.7
	(3)	.702	76.3	28.6
(c)	(1)	.854	5.19	5.19
	(2)	.702	10.44	10.44
	(3)	.425	46.1	27.2
(d)	(1)	.425	2.58	2.58
	(2)	.425	6.94	6.94
	(3)	.425	46.1	27.2

Figure 10: Table of Calculated Buckling Stresses from Actual Channel Dimensions

3.4.6 Reduction of Channel Test Data

Graphs were plotted of applied moment vs. strain for each strain gage of each channel, and were shown in figures 28 and 29, 30 and 31, and 32 and 33 for channels #1, #2, and #3 respectively. Strain gage locations for each channel were shown in figures 28, 30 and 32.

By studying the moment-strain curves and the log sheets, the critical crippling moment and ultimate moment were established for each channel section. Stress distribution curves were plotted to scale for the M_{cr}, M_{ult}, and two other significant moments in figures 35, 36, and 37. Stress was determined from the strain readings by use of Young's modulus

$$\sigma_{(ksi)} = E_{(ksi)} \times \varepsilon_{(microinches)} = 28.6 \times \text{strain}$$

It was noted that gage 5 and gage 1 plotted different moment-strain curves which indicated that the channel was being loaded eccentrically. This error was particularly pronounced in channels #(1) and #(2). At lower loads gage 1 read a greater amount of strain. When a certain intermediate load was reached the channel had deformed sufficiently to fit the loading appartatus, and from that point on each flange took the same amount of strain. At higher loads readings from gage 5 became insignificant due to high bending strains as the flange assumed its buckled shape.

This eccentric loading was compensated for in the following manner as shown in the table of figure 34. In the range of lower loads, before the flanges were accepting an equal amount of applied moment, the actual strain was taken as an average of gages 1 and 5 . This averaging method was used up to the point where the channel had warped sufficiently to no longer load eccentrically. Further incremental loading applied equal stress to each flange. At this point gage 1 showed a higher strain in that flange than gage 5. Half the difference of these two strains was subtracted from the strain readings of gage 1 at all moments above the intermediate moment. Strains from gages 2, 3, and 6 were all adjusted in a proportional manner, depending on the distance from the neutral axis.

The intermediate moment for the different channels was:

Channel #1	2,000 inch lbs.
Channel #2	2,000 inch lbs.
Channel #3	1,000 inch lbs.

The following checks were made of the stress distributions:

1. Using the formula $\sigma = \frac{Mc}{I}$, the extreme fibre stresses were calculated for moments in the elastic range and compared to the measured stresses. (see figure 11)

2. The area of compressive stress equalled the area of tensile stress since thickness was a constant. (see figure 38)

3. The area of compressive stress x flange thickness x moment arm between compressive and tensile

area centroids equalled the applied moment. (see figures 38 and 12)

In the case of channel #3 where the flange strain exceeded the yield strain, the points of stress were plotted in figure 37 as if the material was infinitely elastic. These points were connected by the dotted lines, but the actual stress distribution was shown by the cutoff at σ_{cr}. For the 1,000 inch lb. unloading moment the stress diagram was found by subtracting half of 1,000 inch lb. loading moment diagram from the 1,500 inch lb. diagram. The 1,500 inch lb. diagram was shown dotted.

3.4.7 Determining k at σ_{cr}

The values of M_{cr} were established by studying the test data and moment-strain curves. Test values of k were determined as follows, and plotted on figure 39.

<u>Channel #1</u>: $M_{cr} = 3{,}750$ in-lbs

$$\sigma_{cr} = \frac{M}{S} = \frac{3.75}{.482} = \underline{7.78 \text{ ksi}}$$

$$k = \frac{\sigma_{cr}\, 12(1 - \nu^2)}{\pi^2 E} \left(\frac{b_f}{t_f}\right)^2 = \frac{7.78\ (1.0)}{25.9 \times 10^3} \left(\frac{3.98}{.0610}\right)^2 = \boxed{1.28}$$

Channel #2: $M_{cr} = 3{,}750$ in-lbs

$$\sigma_{cr} = \frac{3.75}{.197} = \underline{19.05 \text{ ksi}}$$

$$\sqrt{\tau} = \sqrt{\frac{(\sigma_y - \sigma_{cr}) \quad \sigma_{cr}}{(\sigma_y - \sigma_p) \quad \sigma_p}} = \sqrt{\frac{(30 - 19.05) \ 19.05}{(30 - 17.7) \ \ 17.7}} = \underline{.98}$$

$$k = \frac{19.4}{25.9 \times 10^3 (.98)} \left(\frac{2.46}{.0618}\right)^2 = \boxed{1.21}$$

Channel #3: $M_{cr} = 1000$ in-lbs

$$\sigma_{cr} = \frac{1000}{.0354} = \underline{28.3 \text{ ksi}}$$

$$\sqrt{\tau} = \sqrt{\frac{(30.0 - 28.3) \ 28.3}{(30.0 - 17.7) \ 17.7}} = \underline{.470}$$

$$k = \frac{28.3}{25.9 \times 10^3 \times (.470)} \left(\frac{.969}{.0628}\right)^2 = \boxed{.554}$$

3.48 Ultimate Moment

A semi-empirical method of predicting ultimate moment was presented in paragraph 5.2 of this report.

3.5 Sources of Error

The chief source of error in the results was the variation of strain gage readings due to eccentric loading. Other sources of error were variations in material thickness, initial eccentricities in flange straightness, inaccuracies in load application at low loads, differences from critical moment in an infinitely long channel and a finite length channel, variations in channel material properties from the tensile test results, inaccuracies in gage and instrument readings, and inability to detect the exact critical load. It was extremely difficult to calculate the exact percent error due to each of these factors. However, it was possible to check the final results in several ways to find the overall percent error.

The main error due to eccentric loading was compensated for by the method explained in paragraph 3.4.6.

By comparing the stresses on the plotted elastic stress distributions (figures 35, 36, and 37) to the calculated stresses a percent error was determined in figure 11.

Channel	Applied Mom. (in. - lbs.)	Calc. Max. Stress = $\frac{M}{S}$(ksi)	Plotted Max. Stress(ksi) (Figs. 35, 36, and 37)	% Error
#1	2,000	4.15	3.7	-10.8
#2	1,000	5.08	5.0	- 1.6
#2	2,000	10.16	9.3	- 8.5
#2	3,750	19.0	18.3	- 3.7
#3	1,000	28.3	30.0	+ 6.0

Figure 11: Table of Percent Error Between Plotted Elastic Stresses and Calculated Elastic Stresses

This error indicated the difference from theoretical elastic stress and strain gage readings. Positive error indicated the plotted stress was higher.

To determine the percent error in the inelastic stress regions, the applied moment was compared to the moment of the stress distribution diagrams. This was done in figure 38 and summarized in figure 12. Positive error indicated the stress diagram moment was higher.

Channel	Applied Mom. (in. - lbs.)	Stress Diagram Moment, (in-lbs)	% Error
#1	3,750	3,390	- 9.6
#1	5,000	4,650	- 7.0
#1	7,000	7,260	+ 3.7
#2	4,750	3,770	-20.6
#3	1,500	1,630	+ 8.7
#3	1,000 (unload)	1,000	0
#3	1,550 (reload)	1,620	+ 4.5

Figure 12: Table of Percent Error Between Calculated Stress Diagram Moments and Actual Applied Moments

The 20.6% error in channel #2 was probably due to an erroneous strain gage reading at the extreme fibre, since this recorded strain was actually lower than the strain at lower moments.

The above errors represented differences from applied moments and strain gage readings. To detect the error in the moment at which buckling occurred was more difficult, and the value could vary as much as 10%. This was especially true in channel #3 which buckled in the inelastic range. Due to dimensional differences and eccentric loading one flange always buckled at a lower load, so it was necessary to interpolate between to get the actual critical moment.

The percent error between the calculated critical stresses of figure 10 using (a), (b), (c) and (d); and the test results were summarized in figure 13. In the inelastic range it was noted that a large variation in the value of k had a small effect on the critical stress. Positive error indicated the test results were higher.

Error in the critical stress due to the flange not being infinitely long was approximated from the case of a uniformly loaded hinged flange. Reference 6 gave for this case the following formula for k;

$$k = .456 + \left(\frac{b}{a}\right)^2 \qquad (16)$$

where:

a = distance between simply supported loaded edges of flange

b = flange width

For the worst case of channel #1 assume

$b = 4.00"$ and $a = 24.0"$

$$k = .456 + \left(\frac{4}{24}\right)^2 = .485$$

$$\%\ \text{Error} = \frac{.485 - .456}{.456} = 6.4\%$$

This estimate was high since the linear varying stress and flange restraint tended to reduce the effective value of b. The effect of the flange length not being infinite was neglected.

Channel	Critical Crippling Stresses (ksi)					% Error			
	Experimental $\sigma_{cr} = \frac{M_{cr}}{S}$	Met. (a)	Met. (b)	Met. (c)	Met. (d)	Met. (a)	Met. (b)	Met. (c)	Met. (d)
#1	7.78	7.91	7.65	5.19	2.58	-1.7	+1.7	+33.3	+67.9
#2	19.05	18.5	16.7	10.44	6.94	+2.9	+12.3	+45.2	+63.6
#3	28.3	29.4	28.6	27.2	27.2	-3.9	-1.1	+ 3.9	+ 3.9

Figure 13: Table of Percent Error Between Calculated Critical Stresses and Experimental Critical Stresses

4.0 Results

The results of this experiment were presented in the following log sheets and graphs:

1. Channel dimensions and section properties (figure 14).
2. Tensile test log sheets (figures 15 through 17).
3. Tensile stress-strain curves (figures 18 through 24).
4. Channel buckling test log sheets (figures 25 through 27).
5. Channel buckling test moment-strain curves (figures 28 through 33).
6. Table to plot stress distribution curves from moment-strain curves (figure 34).
7. Channel buckling test stress distribution curves (figures 35 through 37).
8. Check of stress distribution curves by area and moment balance (figure 38).
9. Values of k vs. b_w/b_f from test results and theoretical methods (a), (b), (c), and (d) (figures 39 and 41).

	Channel #1	Channel #2	Channel #3
f_L	4.01	2.49	1.00
f_F	4.01	2.49	1.01
t_L	.0622	.0620	.0628
t_R	.0610	.0618	.0628
b	4.00	3.99	3.99
$\bar{y}$	2.65	1.762	.810
A	.734	.555	.376
I	1.278	.348	.0287
S	.482	.197	.0354

Figure 14: Channel Dimensions and Section Properties

FIGURE 15

TENSILE TEST LOG SHEETS

SPECIMEN #1

LOAD, P (lbs.)	DIAL READING	DEFL in./in.×10⁶	P/A (PSI)	REMARKS
0	0	0	0	
100	15	75	3,160	LEANNING TEST STAND
200	37	185	6,330	
300	58	290	9,550	
400	79	395	12,660	
500	100	500	15,820	
600	122	610	18,980	
700	152	760	22,200	
800	183	915	25,300	
~~925~~				
~~1445~~ (ULT.)				
900	420	2100	28,500	
925	—	—		YIELD
1445	—	—	45,700	ULT.

$A = .502 \times .063 = .0316 \text{ in.}^2$

SPECIMEN #2

LOAD, P (lbs.)	DIAL READING	DEFL. in./in.×10⁶	~~REMARKS~~ P/A (PSI)	REMARKS
0	0	0	0	
50	7	35	1,560	
100	18	90	3,130	
150	28	140	4,690	
200	39	195	6,250	
250	47	235	7,810	
300	57	285	9,380	
350	71	355	10,920	
400	82	410	12,520	
450	98	490	14,060	
500	109	545	15,610	
550	120	600	17,190	
600	132	660	18,770	
650	147	735	20,300	
700	162?	810	21,900	
750	196	980	23,400	
800	233	1165	25,000	
850	520	2600	26,600	
900	1500	7500	28,100	
1425	—	—	45,600	ULT

$A = .5005 \times .064 = .0320 \text{ in.}^2$

DO NOT USE

DO NOT USE

FIGURE 15 FIGURE 16

TENSILE TEST LOG SHEETS

SPECIMEN #3, A = .5005 × .063 = .0315 in.^{2}

LOAD, P (lbs.)	DIAL READING	DEFL in./in.×10^6	P/A psi	REMARKS
0	0	0	0	
50	8			
100	19			
150	30			
200	40			
250	49			
300	61			
350	77			
400	91			SLIPPED
450	105			
500	119			
550	131			
600	142			
650	158			
700	178			GRIPS
750	—			
800	—			
880	237			
900	290			
1420	2005			ULT.

DO NOT USE

SPECIMEN #4, A = .503 × .0627 = .0315 in.^{2}

LOAD, P (lbs.)	DIAL READING	DEFL in./in.×10^6	P/A (psi)	REMARKS
0	0	0	0	
50	12	60	1,590	
100	20	100	3,180	
150	30	150	4,760	
200	41	205	6,350	
250	55	275	7,940	
300	68	340	9,520	
350	80	400	11,110	
400	91	455	12,700	
450	105	525	14,280	
500	117	585	15,870	
550	128	640	17,460	
600	139	695	19,030	
650	152	760	20,600	
675	161	805	21,900	
700	168	840	22,200	
725	175	875	23,000	
750	181	905	23,800	
775	190	950	24,600	
800	198	990	25,400	
825	203	1015	26,200	
850	211	1055	27,000	
875	225	1125	27,800	
900	240	1200	28,600	
925	460	2300	29,400	
940	650	3255	29,900	
950	830	4150	30,200	
975	1400	7000	31,000	
1485	—	—	47,100	ULT.

FIGURE 16

TENSILE TEST LOG SHEETS

SPECIMEN #5, A = .505 × .0631 = .0319 in.²

LOAD, P (lbs.)	DIAL READING	DEFL. in./in.×10⁶	P/A (psi)	REMARKS
0	0	0	0	
50	6	30	1,570	
100	17	85	3,140	
150	28	140	4,710	
200	38	190	6,290	
250	50	250	7,860	
300	61	305	9,440	
350	72	360	11,000	
400	81	405	12,580	
450	89	445	14,150	
500	101	505	15,720	
550	113	565	17,300	
600	126	630	18,850	
650	139	695	20,400	
675	146	730	21,200	
700	150	750	22,000	
725	157	785	22,800	
750	161	805	23,600	
775	167	835	24,400	
800	172	860	25,200	
825	179	895	25,900	
850	185	925	26,700	
875	189	945	27,500	
900	195	975	28,300	
925	204	1020	29,100	
950	216	1080	29,900	
970	240	1200	30,500	
965	500	2750	30,400	
1495	—	—	46,900	ULT.

SPECIMEN #6, A = .502 × .0627 = .0315 in.²

LOAD, P (lbs.)	DIAL READING	DEFL. in./in.×10⁶	P/A (psi)	REMARKS
0	0	0	0	
50	11	55	1,590	
100	22	110	3,180	
150	33	165	4,760	
200	47	235	6,350	
250	56?	280	7,940	
300	62?	310	9,520	
350	77	385	11,110	
400	91	455	12,700	
450	104	520	14,280	
500	117	585	15,870	
550	131	655	17,460	
600	146	730	19,030	
650	155	775	20,600	
675	160	800	21,400	
700	166	830	22,200	
725	171	855	23,000	
750	180	900	23,800	
775	191	955	24,600	
800	200	1000	25,400	
825	212	1060	26,200	
850	227	1135	27,000	
875	250	1250	27,800	
900	278	1390	28,600	
915	330	1650	29,000	
935	455	2275	29,700	
945	600	3000	30,000	
1495	—	—	47,500	ULT.

FIGURE 17

TENSILE TEST LOG SHEETS

SPECIMEN #7, A = .500 × .0622 = .0311 in.²

LOAD, P (lbs.)	DIAL READING	DEFL in./in.×10⁶	P/A (PSI)	REMARKS
0	0	0	0	
50	9	45	1,610	
100	20	100	3,220	
150	30	150	4,820	
200	42	210	6,430	
250	54	270	8,040	
300	65	325	9,650	
350	75	375	11,250	
400	85	425	12,870	
450	95	475	14,480	
500	108	540	16,070	
550	121	605	17,690	
600	138	690	19,290	
650	152	760	20,900	
700	170	850	22,500	
750	190	950	24,100	
800	210	1050	25,700	
850	235	1175	27,300	
900	325	1675	28,950	
940	390	1950	30,200	
945	620	3100	30,400	
935	1750	8750	30,050	
1465	—	—	47,100	ULT.

SPECIMEN #8, A = .498 × .0623 = .0310 in.²

LOAD, P (lbs.)	DIAL READING	DEFL. in./in.×10⁶	P/A (PSI)	REMARKS
0	0	0	0	
50	10	50	1,610	
100	20	100	3,220	
150	32	160	4,840	
200	42	210	6,450	
250	56	280	8,060	
300	70	350	9,680	
350	80	400	11,290	
400	90	450	12,900	
450	102	510	14,510	
500	120	600	16,110	
550	135	675	17,720	
600	150	750	19,330	
650	168	840	20,950	
700	181	905	22,550	
750	200	1000	24,200	
800	220	1100	25,800	
850	248	1240	27,400	
900	300	1500	29,000	
950	495	2475	30,600	
975	600	3000	31,400	
1000	730	3650	32,200	
1020	860	4300	32,900	
1035	1065	5325	33,400	
1050	1250	6250	33,900	
1062	1470	7350	34,200	
1075	1710	8550	34,700	
1454	—	—	47,000	ULT.

FIGURE 17

TENSILE TEST LOG SHEETS

SPECIMEN #9, $A = .498 \times .0624 = .0310\ in.^2$

LOAD, P (lbs.)	DIAL READING	DEFL. in./in.×10⁶	P/A (psi)	REMARKS
0	0	0	0	
50	9	45	1,610	
100	20	100	3,220	
150	30	150	4,840	
200	40	200	6,450	
250	50	250	8,060	
300	60	300	9,680	
350	75	375	11,290	
400	88	440	12,900	
450	100	500	14,510	
500	111	555	16,110	
550	125	625	17,720	
600	138	690	19,330	
650	150	750	20,950	
700	163	815	22,550	
750	188	940	24,200	
800	220	1100	25,800	
850	265	1325	27,400	
900	410	2050	29,000	
935	660	3300	30,150	
950	910	4550	30,600	
960	1200	6000	30,950	
975	1660	8300	31,400	
1475	—	—	47,600	ULT.

SPECIMEN #10, $A = .500 \times .0622 = .0311\ in.^2$

LOAD, P (lbs.)	DIAL READING	DEFL. in./in.×10⁶	P/A (psi)	REMARKS
0	0	0	0	
50	8	40	1,610	
100	19	85	3,220	
150	30	150	4,820	
200	41	205	6,430	
250	54	270	8,040	
300	68	340	9,650	
350	78	390	11,250	
400	89	445	12,870	
450	100	500	14,480	
500	109	545	16,070	
550	121	605	17,690	
600	138	690	19,290	
650	150	750	20,900	
700	168	840	22,500	
750	188	940	24,100	
800	208	1040	25,700	
850	242	1210	27,300	
890	395	1975	28,600	
910	510	2550	29,250	
925	770	3850	29,750	
932	1240	6200	30,000	
1443	—	—	46,500	ULT.

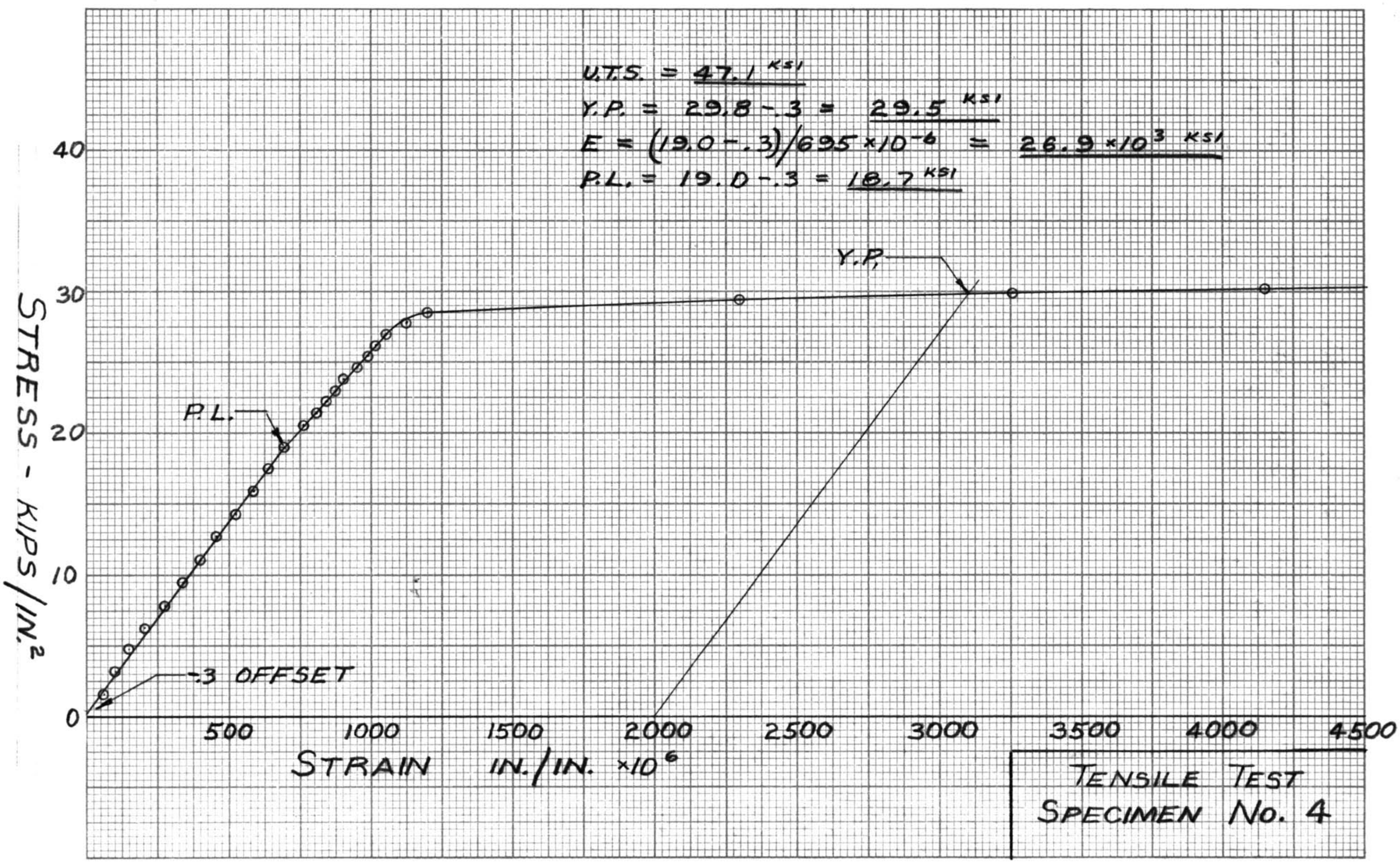
U.T.S. = 47.1 KSI
Y.P. = 29.8 - .3 = 29.5 KSI
E = (19.0 - .3)/695 ×10^-6 = 26.9 ×10^3 KSI
P.L. = 19.0 - .3 = 18.7 KSI
Y.P.
P.L.
.3 OFFSET
STRESS - KIPS/IN.²
STRAIN IN./IN. ×10^6
0
10
20
30
40
500
1000
1500
2000
2500
3000
3500
4000
4500
TENSILE TEST
SPECIMEN No. 4

Figure 18

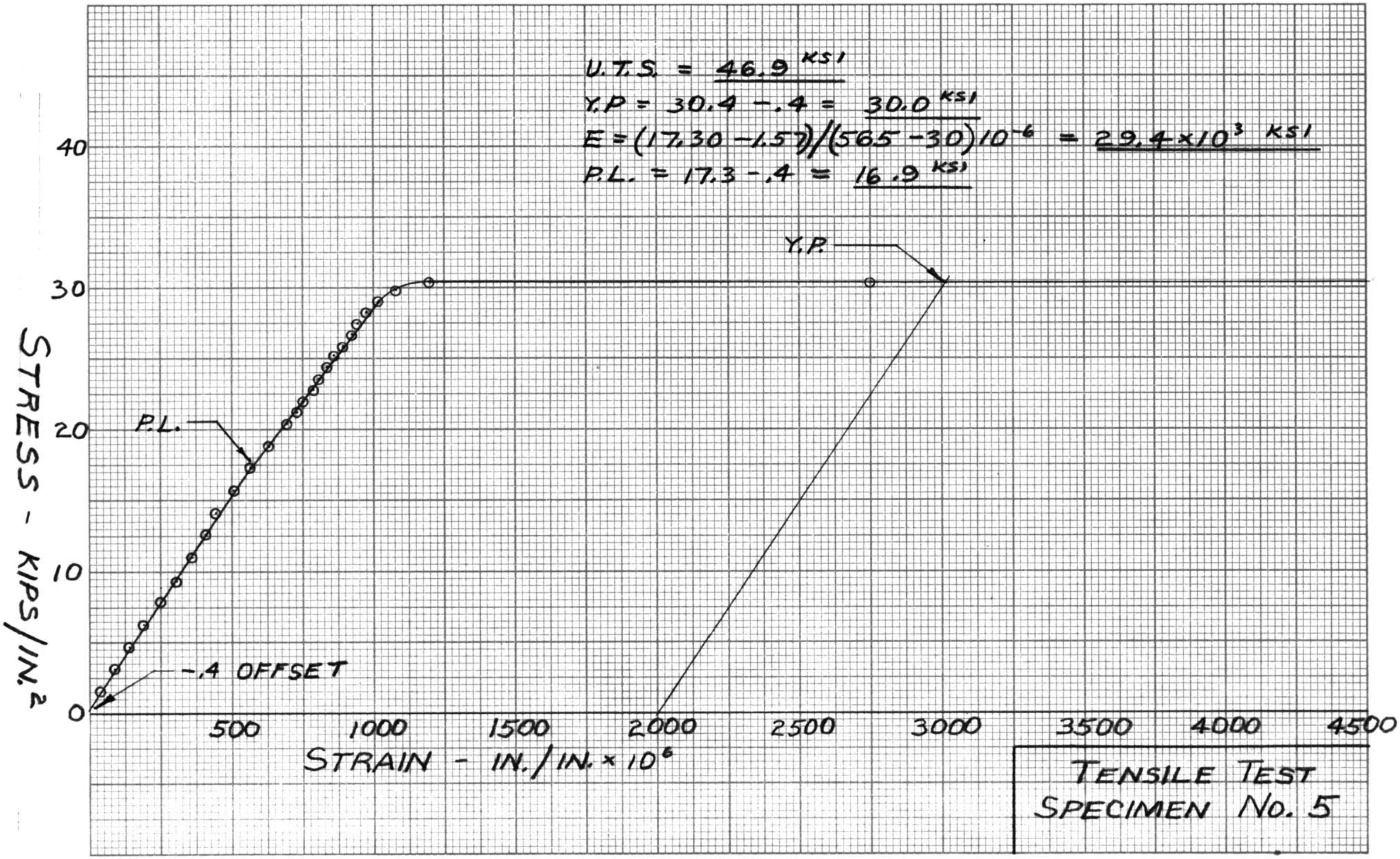
U.T.S. = 46.9 KSI
Y.P = 30.4 − .4 = 30.0 KSI
E = (17.30 − 1.57)/(565 − 30)10⁻⁶ = 29.4×10³ KSI
P.L. = 17.3 − .4 = 16.9 KSI
Y.P.
P.L.
−.4 OFFSET
STRESS - KIPS/IN.²
0
10
20
30
40
500
1000
1500
2000
2500
3000
3500
4000
4500
STRAIN - IN./IN. × 10⁶
TENSILE TEST
SPECIMEN No. 5

Figure 19

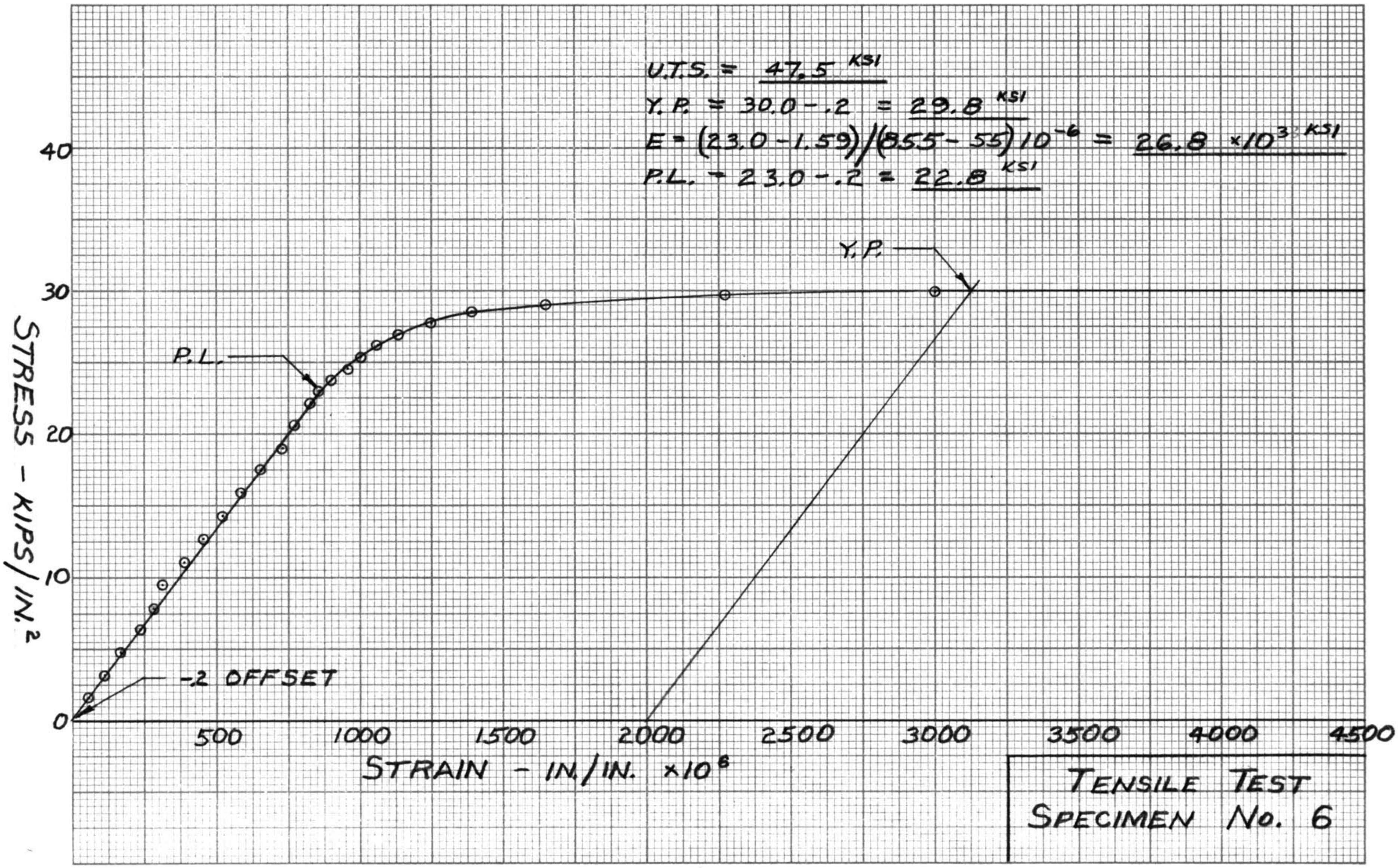
U.T.S. = 47.5 KSI
Y.P. = 30.0 − .2 = 29.8 KSI
E = (23.0 − 1.59)/(855 − 55) 10⁻⁶ = 26.8 ×10³ KSI
P.L. = 23.0 − .2 = 22.8 KSI
Y.P.
P.L.
.2 OFFSET
STRESS − KIPS/IN.²
0
10
20
30
40
500
1000
1500
2000
2500
3000
3500
4000
4500
STRAIN − IN./IN. ×10⁶
TENSILE TEST
SPECIMEN No. 6

Figure 20

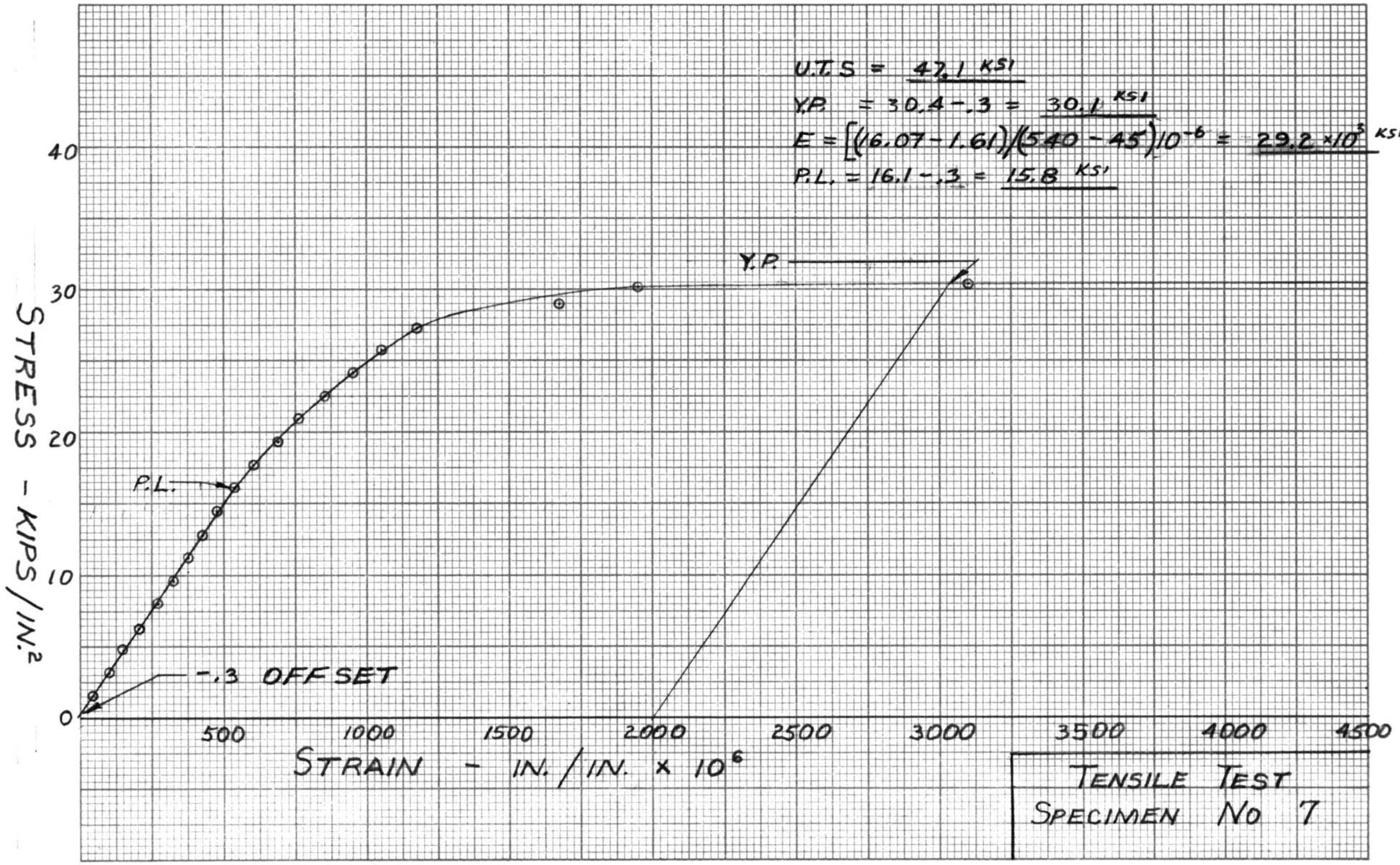
U.T.S = 47.1 KSI
Y.P. = 30.4 − .3 = 30.1 KSI
E = [(16.07 − 1.61)/(540 − 45)]10⁻⁶ = 29.2 ×10³ KSI
P.L. = 16.1 − .3 = 15.8 KSI
Y.P.
P.L.
−.3 OFFSET
0
10
20
30
40
500
1000
1500
2000
2500
3000
3500
4000
4500
STRESS - KIPS/IN.²
STRAIN - IN./IN. × 10⁶
TENSILE TEST
SPECIMEN No 7

Figure 21

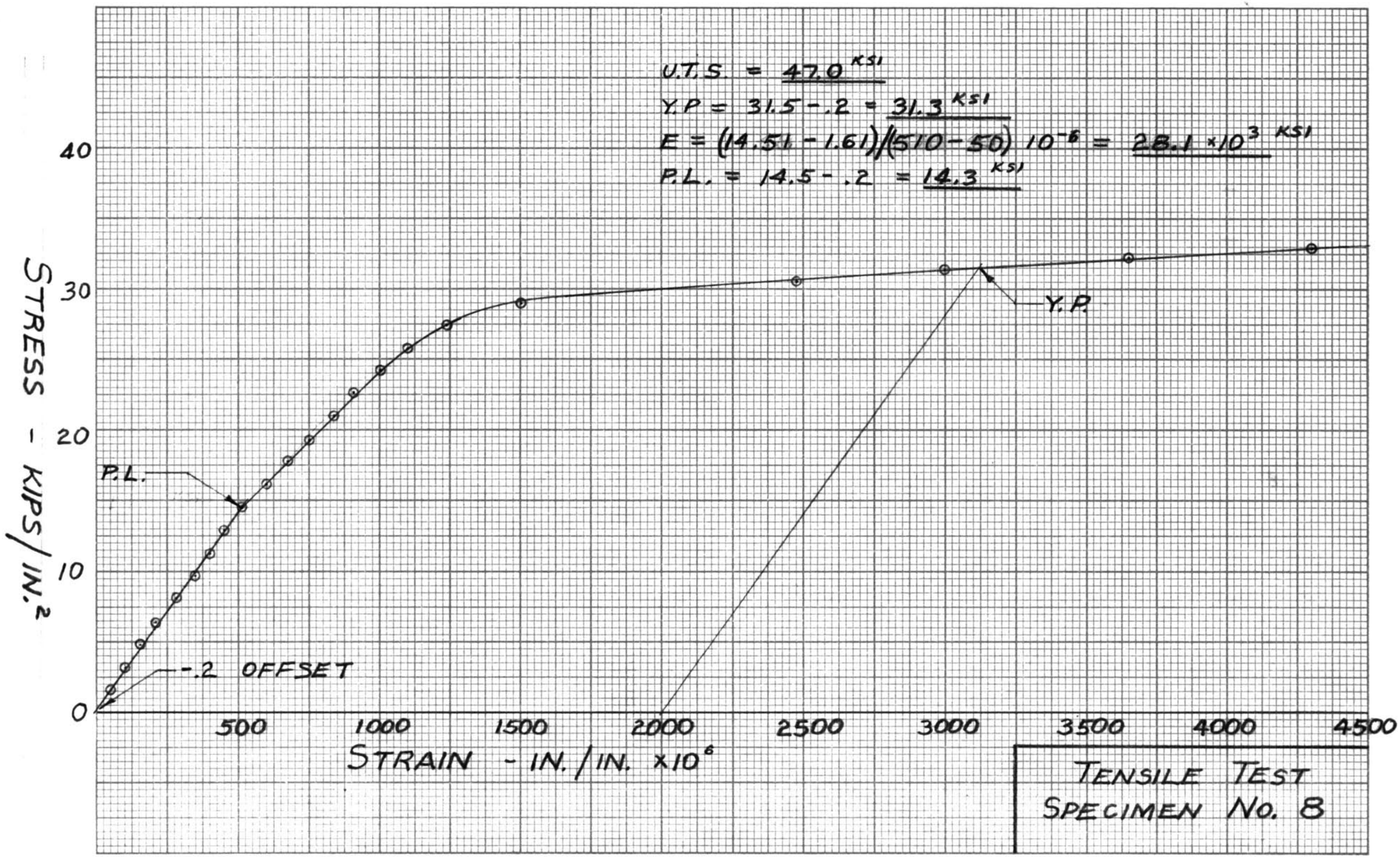

U.T.S. = 47.0 KSI
Y.P = 31.5 - .2 = 31.3 KSI
E = (14.51 - 1.61)/(510 - 50) 10⁻⁶ = 28.1 ×10³ KSI
P.L. = 14.5 - .2 = 14.3 KSI
STRESS - KIPS/IN.²
STRAIN - IN./IN. ×10⁶
P.L.
Y.P.
-.2 OFFSET
0
10
20
30
40
500
1000
1500
2000
2500
3000
3500
4000
4500
TENSILE TEST
SPECIMEN No. 8

Figure 22

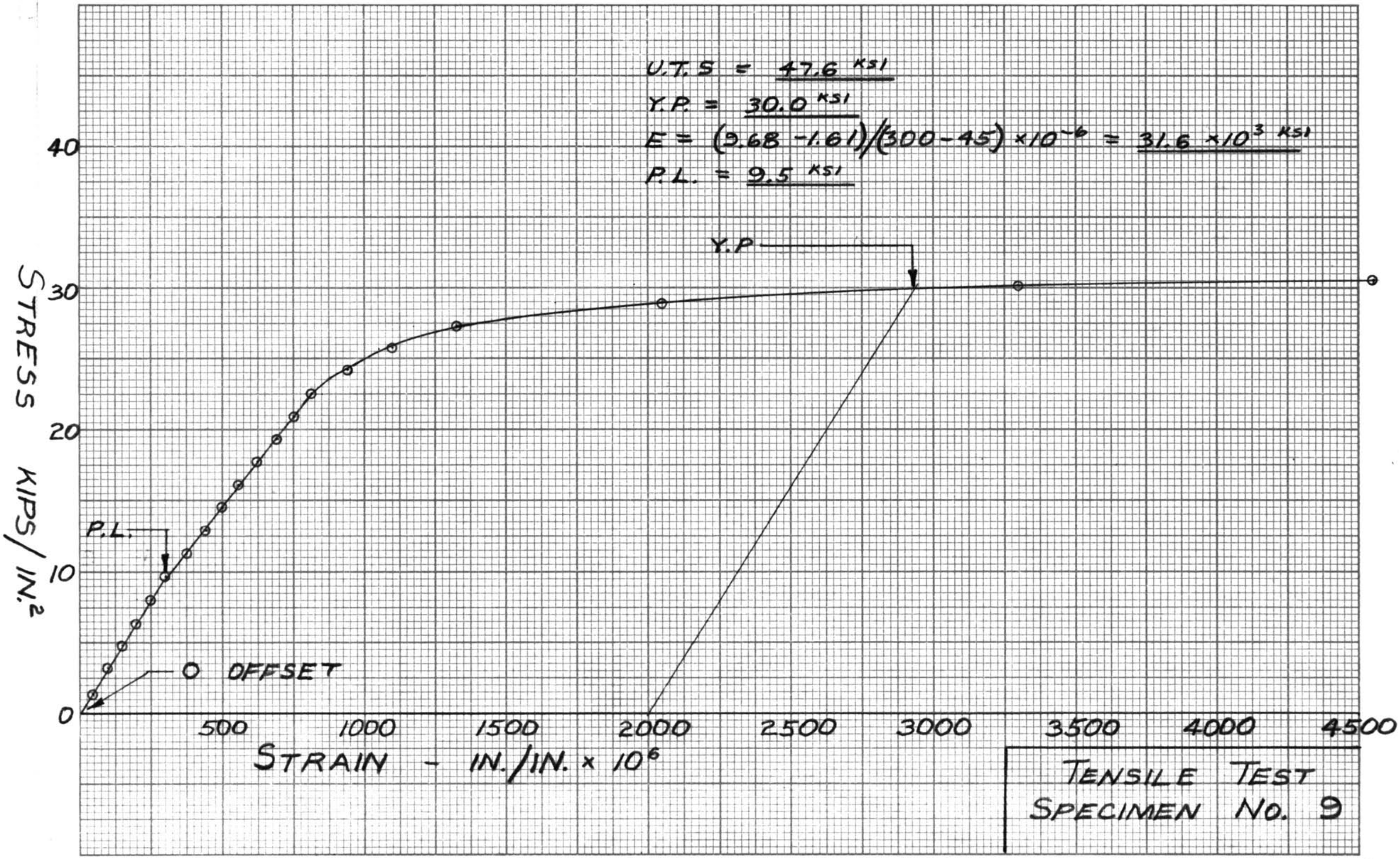
U.T.S = 47.6 KSI
Y.P. = 30.0 KSI
E = (9.68 - 1.61)/(300 - 45) × 10^-6 = 31.6 × 10^3 KSI
P.L. = 9.5 KSI
Y.P
P.L.
O OFFSET
40
30
20
10
0
500
1000
1500
2000
2500
3000
3500
4000
4500
STRESS KIPS/IN.²
STRAIN - IN./IN. × 10^6
TENSILE TEST
SPECIMEN NO. 9

Figure 23

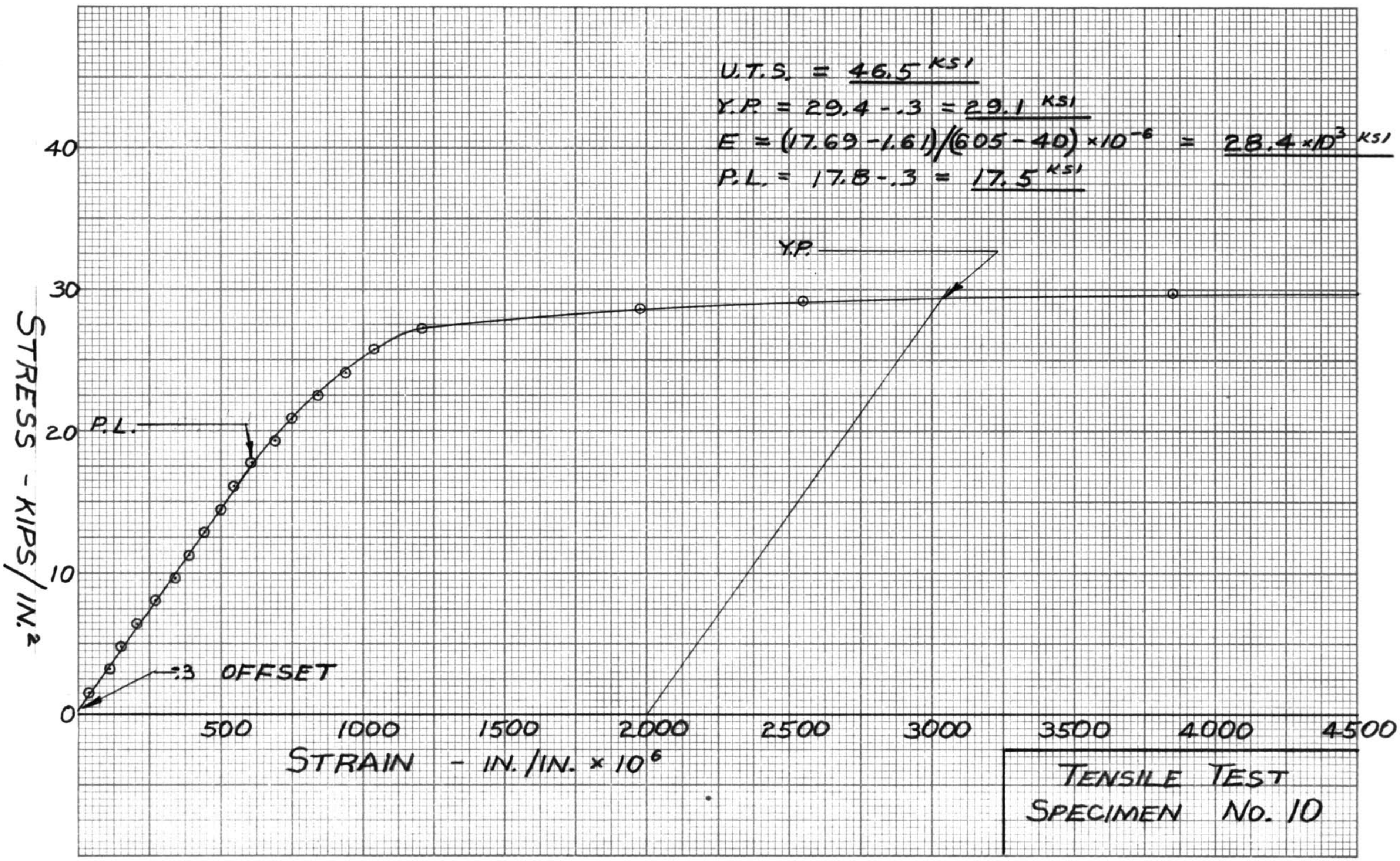
U.T.S. = 46.5 KSI
Y.P. = 29.4 - .3 = 29.1 KSI
E = (17.69 - 1.61)/(605 - 40) × 10⁻⁶ = 28.4 × 10³ KSI
P.L. = 17.8 - .3 = 17.5 KSI
Y.P.
P.L.
.3 OFFSET
STRESS - KIPS/IN.²
STRAIN - IN./IN. × 10⁶
0
10
20
30
40
500
1000
1500
2000
2500
3000
3500
4000
4500
TENSILE TEST
SPECIMEN No. 10

Figure 24

FIGURE 25

LOG SHEET - CHANNEL #1

LOAD, P (lbs.)	MOM. (in.-lbs.)	GAGE READINGS ①	②	③	④	⑤	REMARKS
50	250	5190	5387	5993	7674	5988	
100	500	5167	5372	5992	7657	5982	APPARENTLY
200	1000	5120	5348	5992	7671	5976	LOADING ECCEN-
300	1500	5068	5321	5992	7662	5959	TRICALLY
400	2000	5023	5297	5993	7664	5941	
500	2500	4991	5280	5996	7668	5922	BUCKLE STARTS - GA ① SIDE
600	3000	4960	5255	5996	7662	5893	
700	3500	4945	5239	5991	7659	5870	
750	3750	4927	5230	5986	7662	5860	BUCKLE STARTS - GA ⑤ SIDE
800	4000	4930	5224	5982	7684	5862	
850	4250	4921	5213	5972	7690	5876	
900	4500	4920	5206	5967	7670	5911	
950	4750	4911	5194	5953	7681	5967	
1000	5000	4902	5181	5941	7700	6026	BUCKLE - 1 MODE, 15" LONG
1050	5250	4910	5174	5931	7666	6113	
1100	5500	4910	5158	5908	7659	6181	
1200	6000	4912	5129	5871	7680	6347	
1300	6500	4916	5089	5810	7673	—	
1400	7000	4916	5063	5769	7676	—	
1450	7250	—	—	—	—	—	ULT.

LOADING BEAM WT. = 40#

CHANNEL WT. = 10#

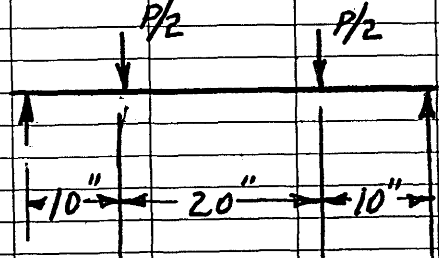

FIGURE 26

LOG SHEETS - CHANNEL #2

LOAD, P (lbs.)	MOM. (in.-lbs.)	GAGE READINGS ①	②	③	④	⑤	⑥	REMARKS
47	235	5128	4181	5096	3826	5724	3690	
150	750	5012	4129	5108	3857	5681	3743	
250	1250	4901	4077	5110	3890	5671	3789	
350	1750	4805	4035	5118	3911	5600	3833	
450	2250	4724	3998	5122	3953	5549	3869	
300	1500	4852	4060	5129	3909	5636	3812	
550	2750	4638	3958	5128	3991	5485	3911	
650	3250	4552	3921	5131	4026	5411	3951	BUCKLE STARTS - GAGE ① SIDE
700	3500	4498	3899	5132	4055	5360	3968	
750	3750	4488	3878	5118	4090	5268	3981	BUCKLE STARTS - GAGE ⑤ SIDE
800	4000	4499	3860	5101	4124	5161	3983	
450	2250	4712	4003	5122	3963	5520	3867	
550	2750	4632	3964	5124	4000	5444	3904	BUCKLE STARTS - GAGE ① SIDE
650	3250	4562	3929	5129	4039	5360	3933	
700	3500	4530	3908	5118	4066	5297	3950	
750	3750	4513	3887	5110	4090	5231	3964	SLIGHT BUCKLE STARTS GAGE ⑤ SIDE
800	4000	4510	3863	5099	4117	5152	3978	
850	4250	4519	3843	5081	4148	5051	3986	BUCKLE - 2 MODES - 9" LONG
900	4500	4542	3818	5057	4183	4911	3992	
950	4750	4628	3802	5016	4242	4846	3968	ULT.

LOADING BEAM WT. = 40#

CHANNEL WT. = 7#

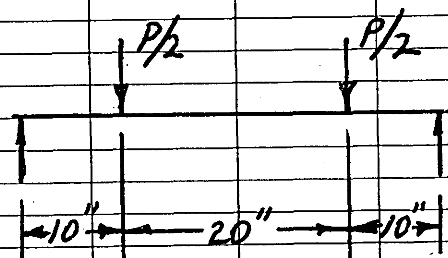

FIGURE 27

LOG SHEETS - CHANNEL #3

LOAD, P (lbs.)	MOM. (in.-lbs.)	GAGE READINGS ①	②	④	⑤	⑥	REMARKS
45	225	4719	4936	7587	6378	2552	
100	500	4509	4938	7649	6190	2621	
120	600	4411	4937	7681	6108	2648	
140	700	4329	4937	7701	6038	2671	
160	800	4249	4933	7726	5969	2688	
100	500	4471	4937	7652	6182	2621	
160	800	4239	4934	7722	5959	2690	
180	900	4151	4931	7740	5889	2710	
200	1000	4041	4928	7763	5780	2734	
220	1100	3929	4918	7791	5630	2760	
240	1200	3833	4909	7822	5423	2790	
260	1300	3730	4890	7858	5137	2810	
280	1400	3596	4849	7898	4483	2842	
300	1500	3121	4702	7978	2169	2920	
200	1000	3479	4698	7869	2621	2803	
260	1300	3243	4698	7937	2339	2878	
310	1550	2341	4581	8047	B 8118	3003	ULT. - BUCKLE, 1 MODE - 1 1/4" LONG

LOADING BEAM WT. = 40#

CHANNEL WT. = 5#

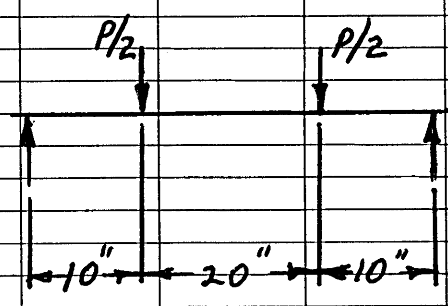

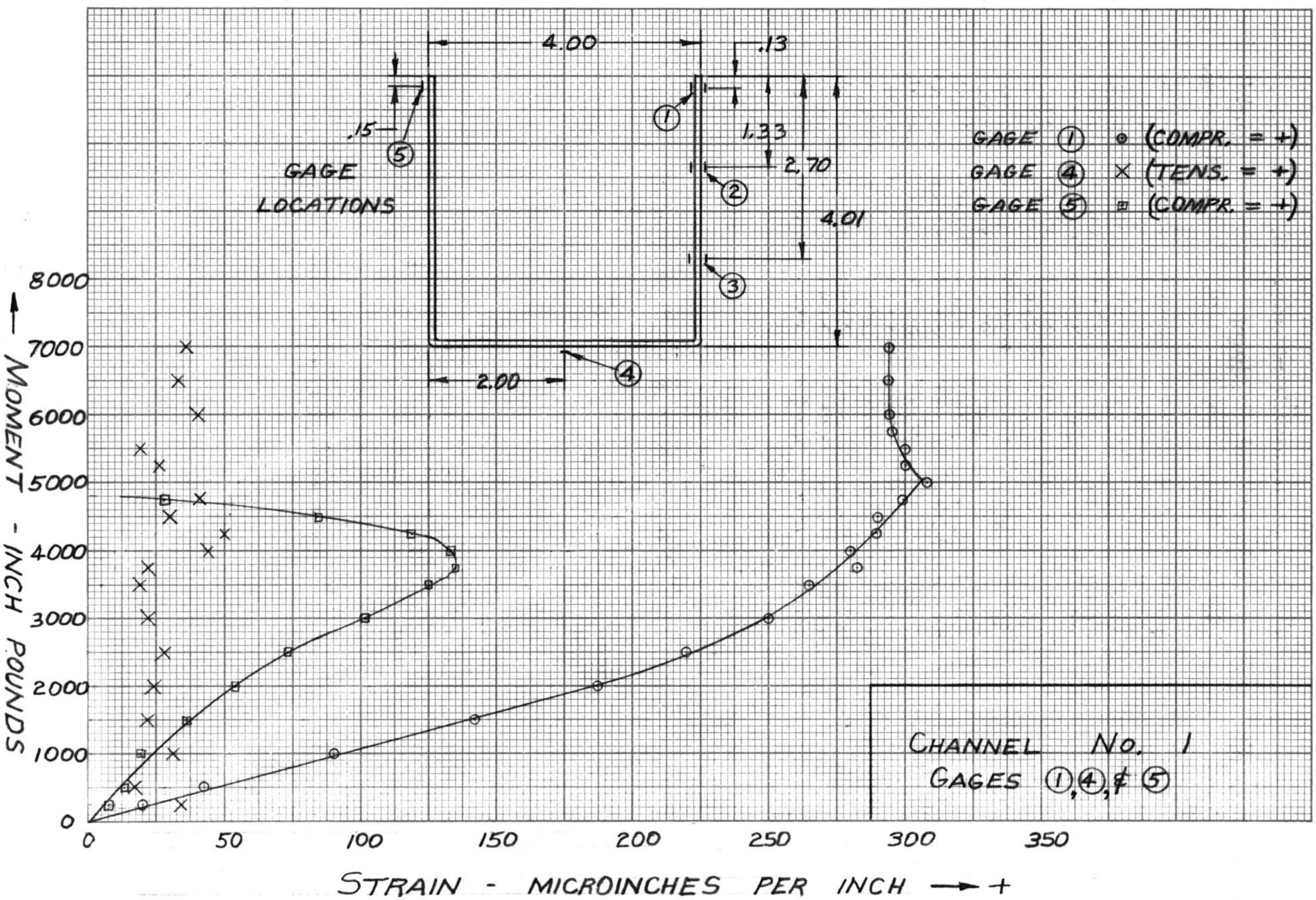
4.00
.13
.15
5
1
1.33
2.70
2
4.01
3
2.00
4
GAGE LOCATIONS
GAGE 1 ⊙ (COMPR. = +)
GAGE 4 × (TENS. = +)
GAGE 5 ⊡ (COMPR. = +)
CHANNEL NO. 1
GAGES 1, 4, & 5
MOMENT - INCH POUNDS
8000
7000
6000
5000
4000
3000
2000
1000
0
0
50
100
150
200
250
300
350
STRAIN - MICROINCHES PER INCH → +

Figure 28

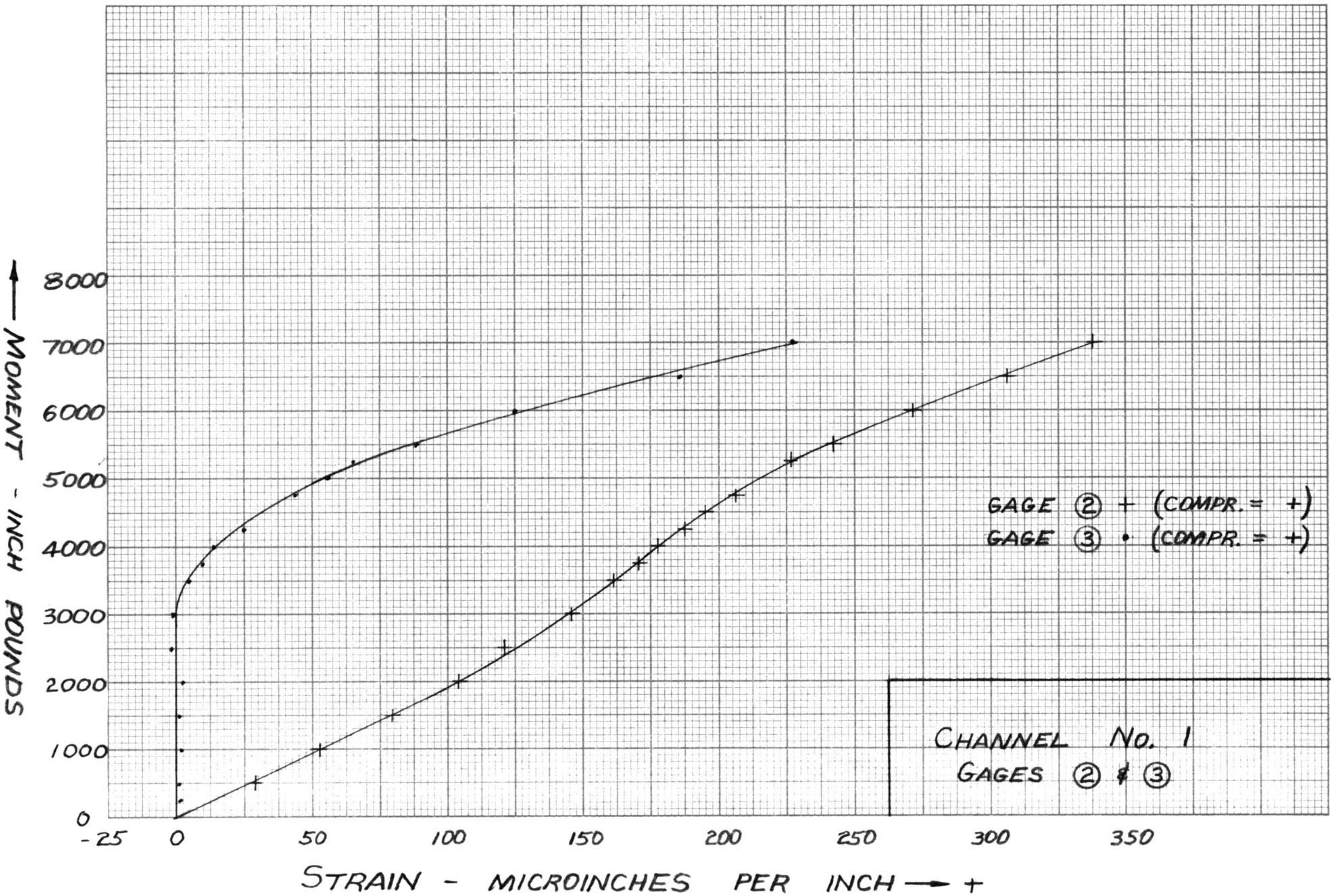
MOMENT - INCH POUNDS
8000
7000
6000
5000
4000
3000
2000
1000
0
-25
0
50
100
150
200
250
300
350
STRAIN - MICROINCHES PER INCH → +
GAGE ② + (COMPR. = +)
GAGE ③ • (COMPR. = +)
CHANNEL No. 1
GAGES ② & ③

Figure 29

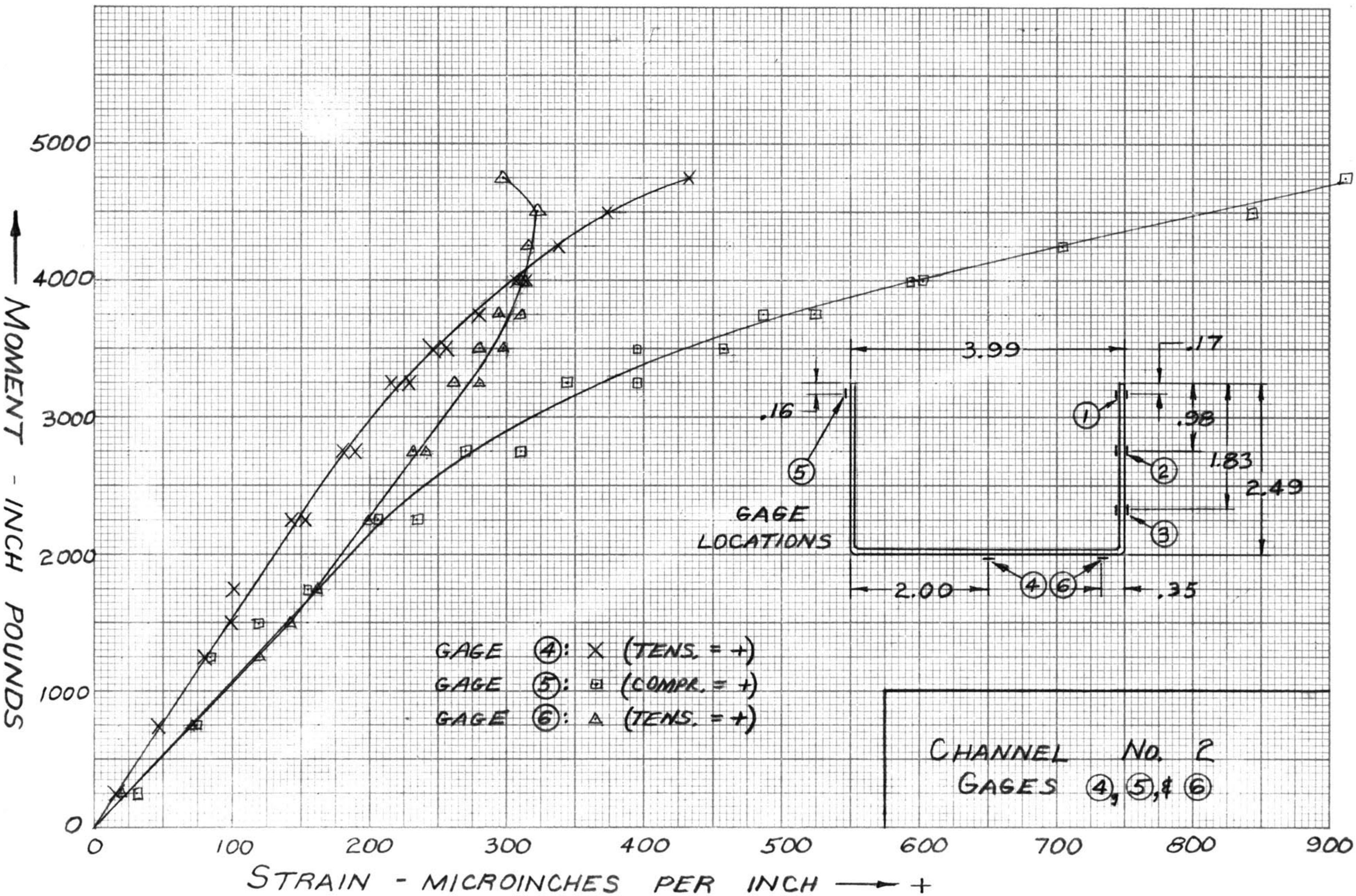
MOMENT - INCH POUNDS
STRAIN - MICROINCHES PER INCH → +
0
1000
2000
3000
4000
5000
0
100
200
300
400
500
600
700
800
900
GAGE ④: × (TENS. = +)
GAGE ⑤: ⊡ (COMPR. = +)
GAGE ⑥: △ (TENS. = +)
GAGE LOCATIONS
3.99
.17
.16
.98
1.83
2.49
2.00
.35
1
2
3
4
5
6
CHANNEL No. 2
GAGES ④, ⑤, & ⑥

Figure 30

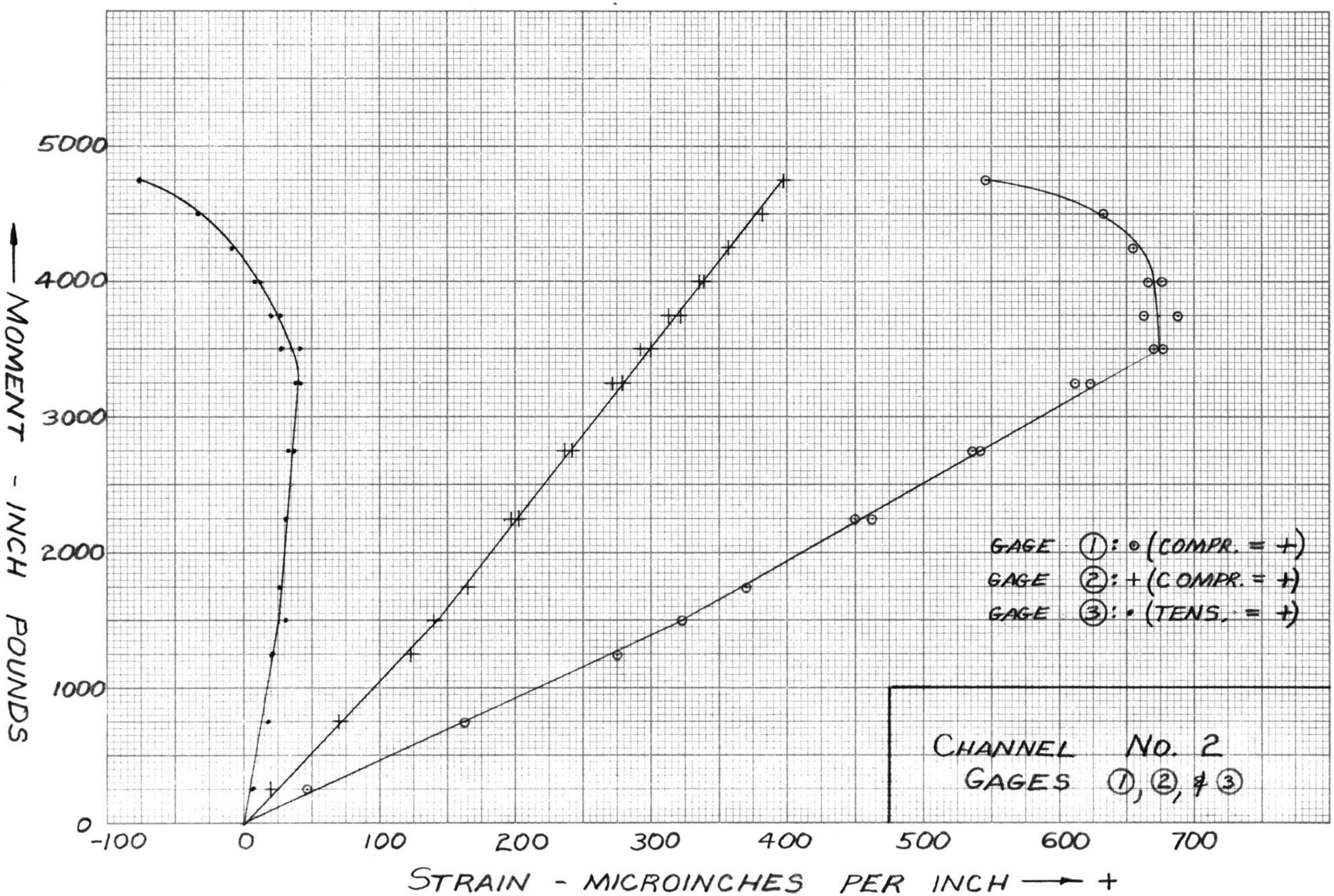

MOMENT - INCH POUNDS
STRAIN - MICROINCHES PER INCH → +
GAGE ①: ⊙ (COMPR. = +)
GAGE ②: + (COMPR. = +)
GAGE ③: • (TENS. = +)
CHANNEL NO. 2
GAGES ①, ②, & ③

Figure 31

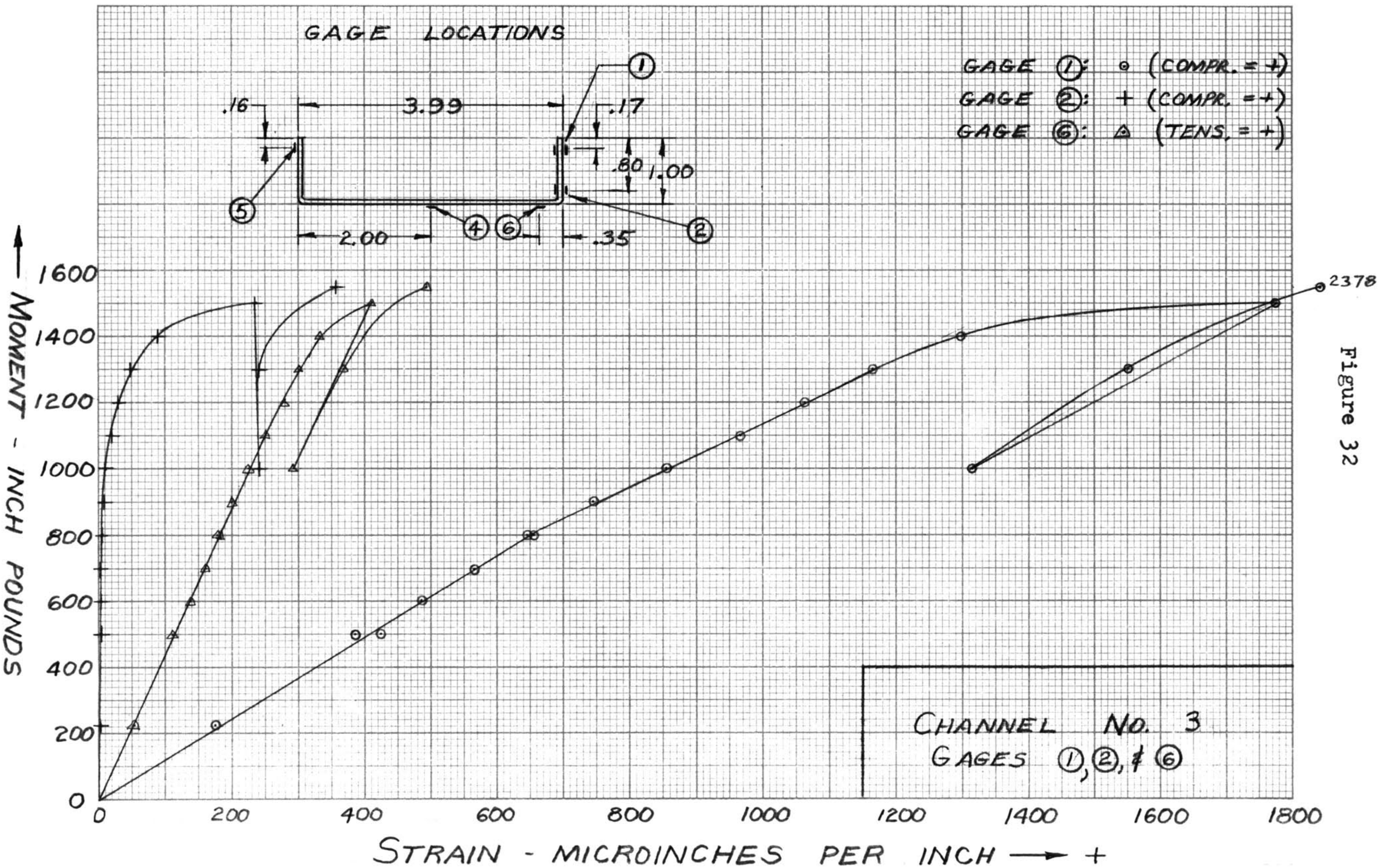
GAGE LOCATIONS
.16
3.99
.17
.80
1.00
2.00
.35
1
2
4
5
6
GAGE ①: ⊙ (COMPR. = +)
GAGE ②: + (COMPR. = +)
GAGE ⑥: △ (TENS. = +)
2378
CHANNEL NO. 3
GAGES ①, ②, & ⑥
MOMENT - INCH POUNDS
0
200
400
600
800
1000
1200
1400
1600
1800
STRAIN - MICROINCHES PER INCH → +

Figure 32

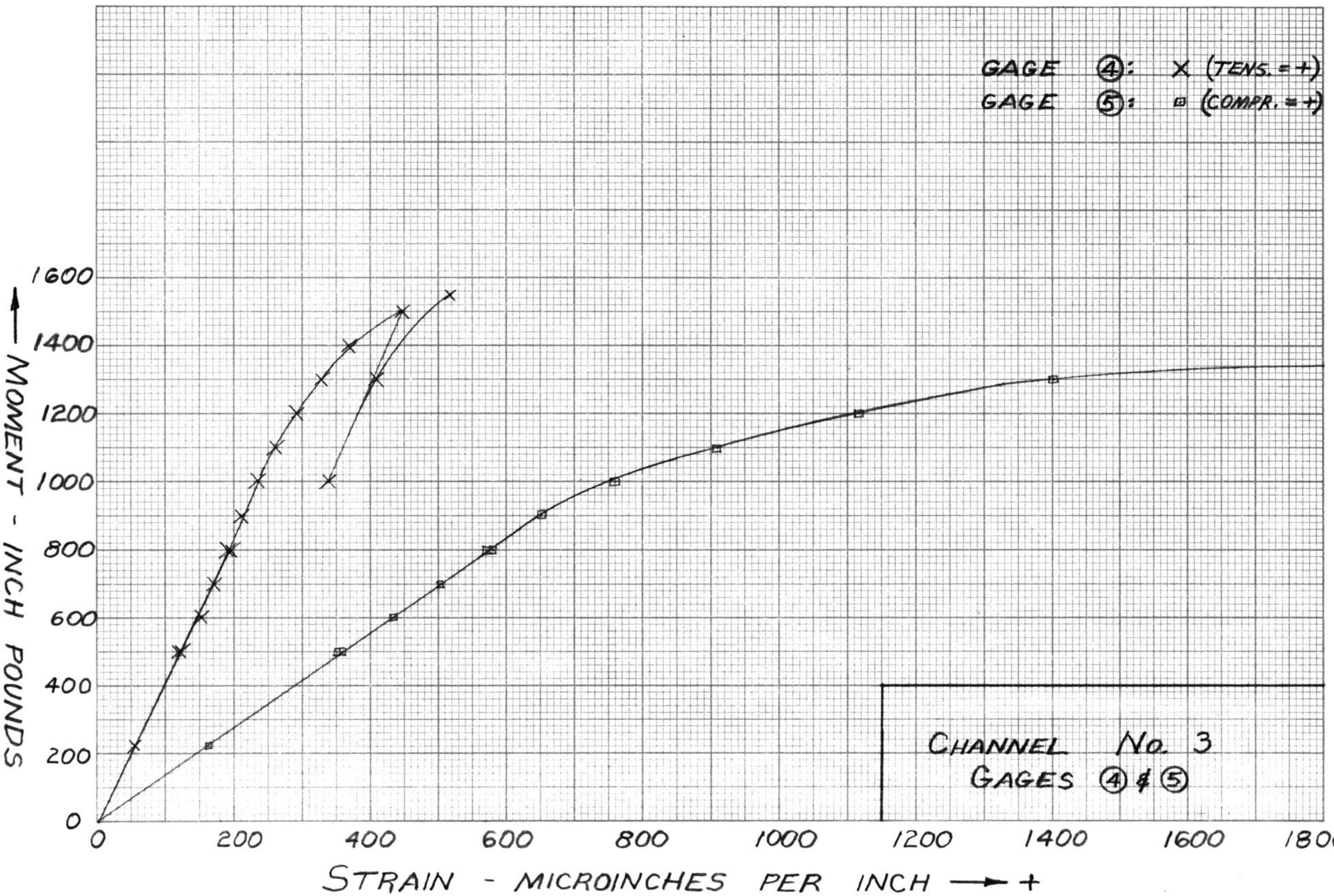
GAGE ④: X (TENS. = +)
GAGE ⑤: ⊡ (COMPR. = +)
CHANNEL No. 3
GAGES ④ & ⑤
MOMENT - INCH POUNDS
0
200
400
600
800
1000
1200
1400
1600
0
200
400
600
800
1000
1200
1400
1600
1800
STRAIN - MICROINCHES PER INCH → +

Figure 33

Moment	Strain at outer fibres: Gage 1	Gage 2	$\frac{1-2}{2}$	Modi. Strn. Gage 1 factor	Modified Strain, Gage 1	Gage 1 Stress (ksi)	Gage 2: Strain	Factor	Modified Strain Gage 2	Gage 2 Stress (ksi)	Gage 3: Strain	Factor	Modified Strain Gage 3	Gage 3 Stress (ksi)	Gage 4: Strain	Factor	Modified Strain Gage 4	Gage 4 Stress (ksi)	Gage 6: Strain	Factor	Modified Strain Gage 6	Gage 6 Stress (ksi)
CHANNEL #1	$E = 28.6 \times 10^3$ ksi																					
2000	187	54	-66	(-.65)	121	3.46	104	(.65)	68	1.95	0	0	0	0	-	-	-	-				
3750 M_{cr}	275	-	-66	-	209	5.98	170	-36	134	3.83	9	0	9	.27	-	-	-	-				
5000	306	-	-66	-	240	6.87	216	-36	180	5.15	54	0	54	1.54	-	-	-	-				
7000	294	-	-66		228	6.52	338	-36	302	8.63	228	0	228	6.52	-	-	-	-				
CHANNEL #2	$E = 28.6 \times 10^3$ ksi																					
1000	217	94	-61	(.72)	156	4.46	95	(.72)	68	1.95	17	(.72)	12	.34	65	-	65	1.86	95	(.72)	68	1.95
2000	411	186	-112	(.73)	299	8.55	182	(.73	133	3.81	30	(.73)	22	.63	131	-	131	3.75	180	(.73)	123	3.52
3750 M_{cr}	673	561	-112	-	617	17.65	319	-49	270	7.72	25	-8	17	.49	274	-	274	7.84	303	-57	246	7.04
4750	546	-	-112	-	434	12.40	398	-49	349	9.98	(compr) -76	-8	-84	-2.40	433		433	12.38	298	-57	241	6.90
CHANNEL #3	$E = 28.6 \times 10^3$ ksi																					
1000	859	675	- 92	(.90)	767	21.9	9	(.90)	8	.23					237	-	237	6.79	228	(.90)	205	5.86
1500	1777	-	- 92	-	1685	48.2	236	- 1	235	6.73					410	-	410	11.72	448	-23	425	12.16
1000 (unload)	1316	-	- 92	-	1224	35.0	241	- 1	240	6.87					293	-	293	8.39	340	-23	317	9.07
1550 (reload)	2378	-	- 92	-	2286	65.5	358	- 1	357	10.20					493		493	14.09	518	-23	495	14.06

Figure 34: Table to Plot Stress Distribution Curves from Moment-Strain Curves

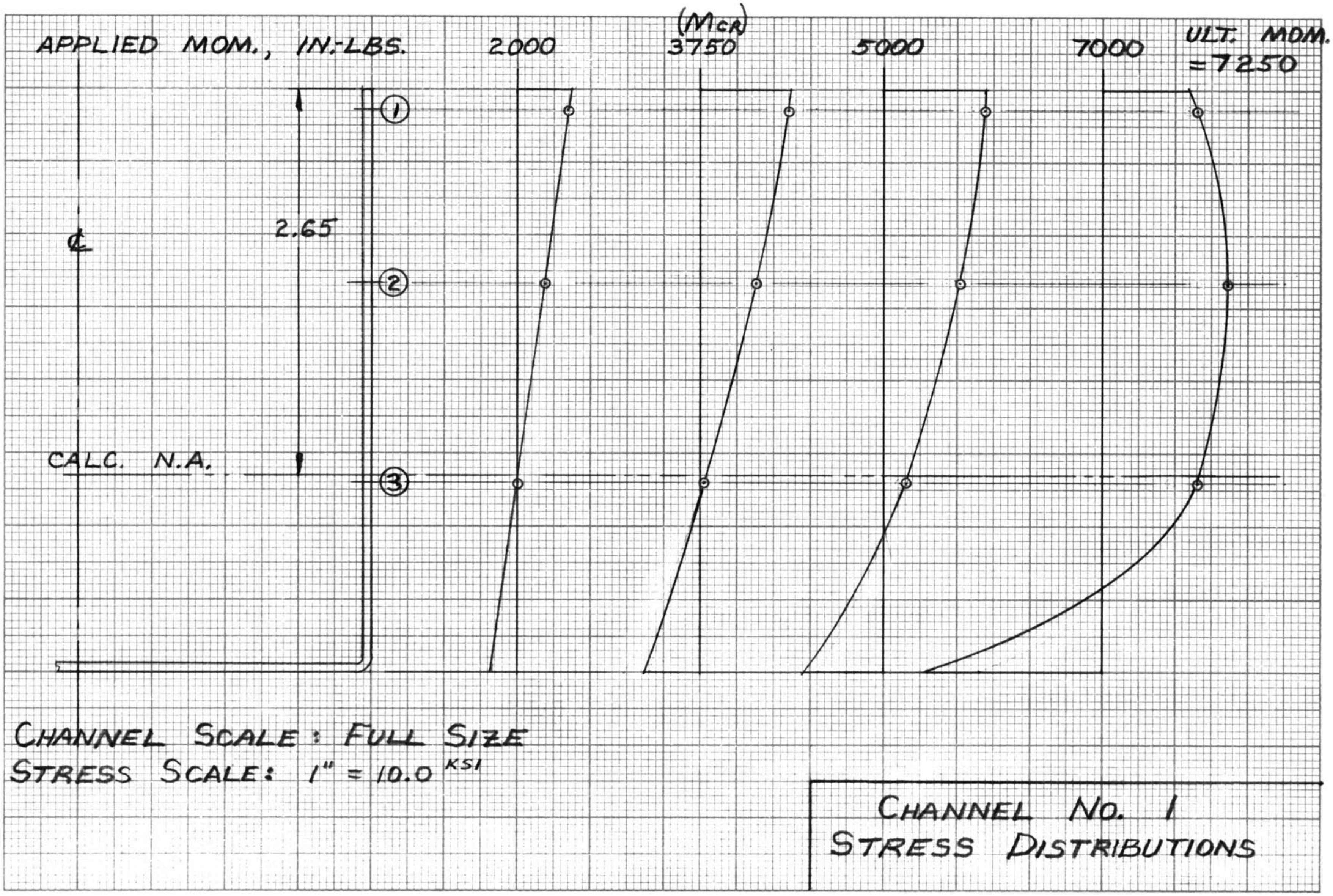

APPLIED MOM., IN.-LBS.
2000
(MCR)
3750
5000
7000
ULT. MOM.
=7250
1
2
3
2.65
℄
CALC. N.A.
CHANNEL SCALE: FULL SIZE
STRESS SCALE: 1" = 10.0 KSI
CHANNEL NO. 1
STRESS DISTRIBUTIONS

Figure 35

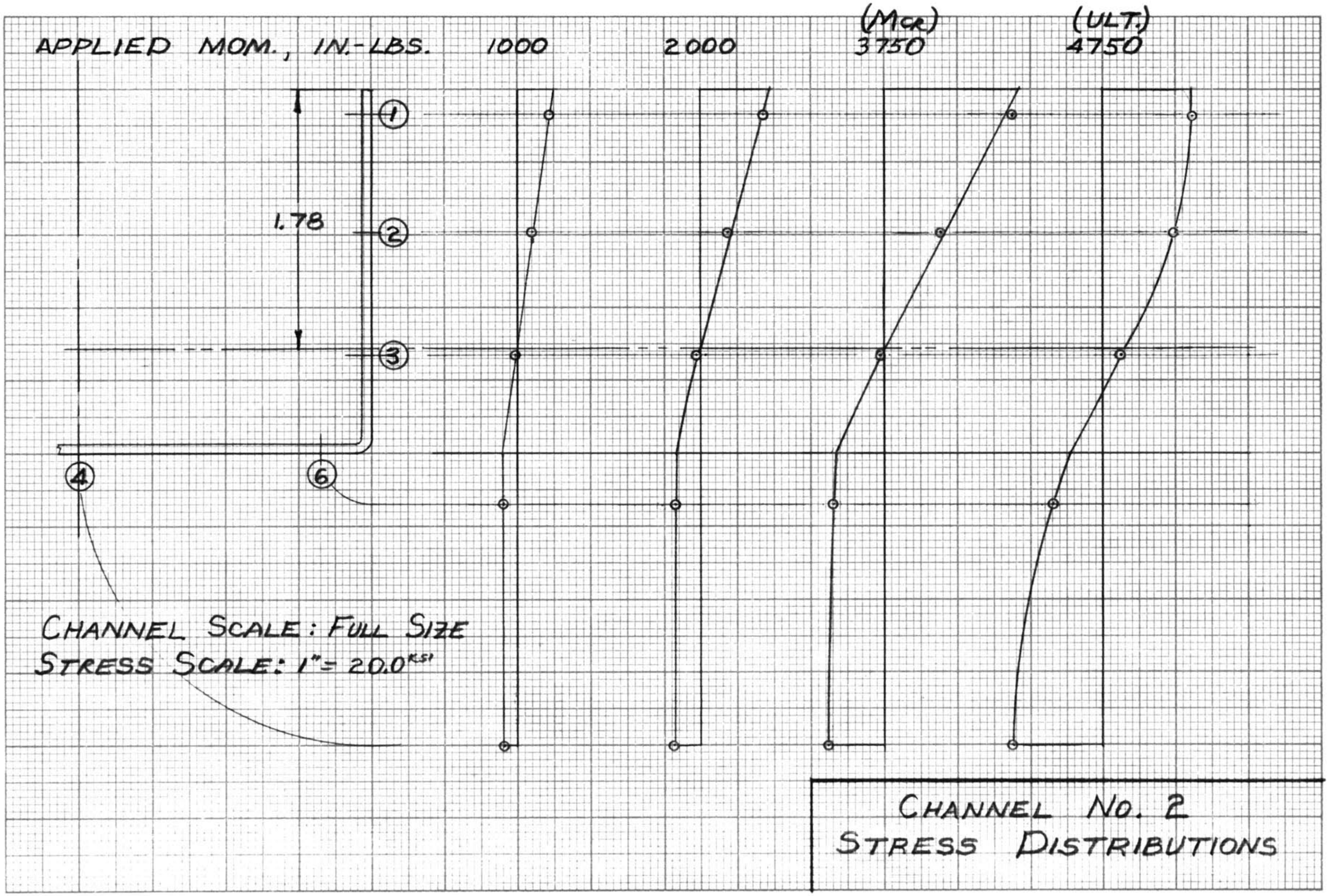

APPLIED MOM., IN.-LBS.
1000
2000
(Mcr)
3750
(ULT.)
4750
1.78
1
2
3
4
6
CHANNEL SCALE: FULL SIZE
STRESS SCALE: 1" = 20.0 KSI
CHANNEL NO. 2
STRESS DISTRIBUTIONS

Figure 36

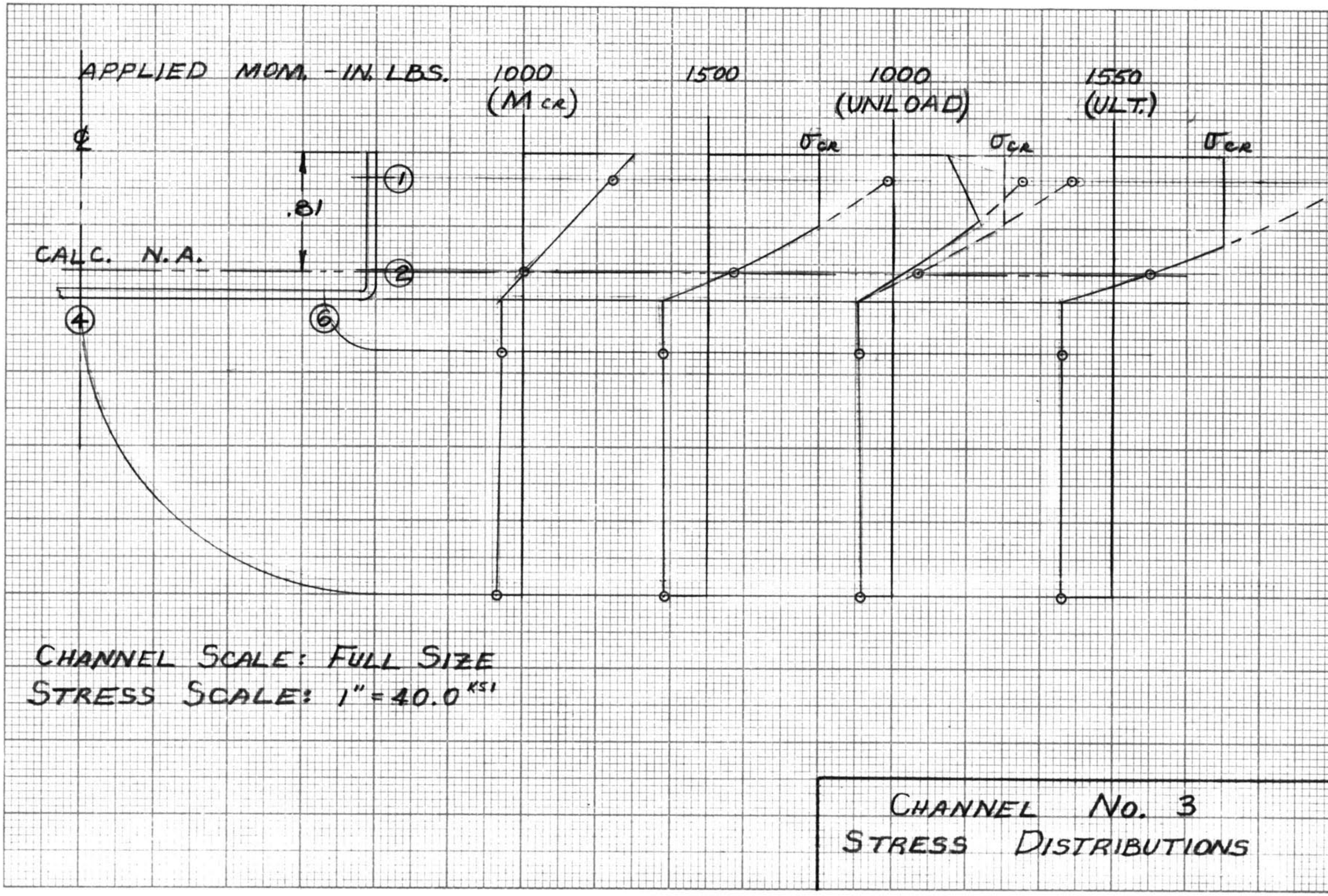
APPLIED MOM. - IN. LBS.
1000
(M cr)
1500
1000
(UNLOAD)
1550
(ULT.)
σ_{cr}
σ_{cr}
σ_{cr}
.81
CALC. N.A.
1
2
4
6
CHANNEL SCALE: FULL SIZE
STRESS SCALE: 1" = 40.0 KSI
CHANNEL No. 3
STRESS DISTRIBUTIONS

Figure 37

Channel	Moment Applied (in.-lbs)			
1	2000	A Compr.	(2.70x3.7/2)2	10.0
		A Tension	(4.01+1.24)1.8	9.8
		Moment	10.0 x .061(1.80+1.21)10^3	1,840
	3750	A Compr.	(2.80x6.9/2)2	19.3
		A Tension	(4.01+1.14)3.8	19.6
		Moment	19.3x.061x2.88x10^3	3,390.
	5000	A Compr.	(3.08x8.6/2)2	26.5
		A Tension	(4.01+.86)5.5	24.8
		Moment	26.5x.061x2.88x10^3	4,650.
	7000	A Compr.	[3.00(10.2+5.0)/2]	45.7
		A Tension	4.01x11.4	45.9
		Moment	45.7x.061x2.55x10^3	7,260.
2	1000	A Compr.	(1.78x5.0/2)2	8.91
		A Tension	(3.99+.65)1.9	8.81
		Moment	8.91x1.80x.0618x10^3	990.
	2000	A Compr.	(1.78x9.3/2)2	16.6
		A Tension	(3.99+.65)3.4	15.8
		Moment	16.6x.0618x1.80x10^3	1840.
	3750	A Compr.	(1.78x18.3/2)2	32.6
		A Tension	4.64x7.0	32.5
		Moment	32.6x.0618x1.80x10^3	3,630
	4750	A Compr.	(2.08x16.3/2)2	33.9
		A Tension	2.42x16.0	38.7
		Moment	33.9x1.80x.0618x10^3	3,770.
3	1000	A Compr.	(.83x30.0/2)2	24.9
		A Tension	6.3x2.05x2	25.8
		Moment	24.9x.0628x.65x10^3	1,010
	1500	A Compr.	2[(.87+.51)/2]30.0	41.4
		A Tension	12.0x2.03x2	48.8
		Moment	41.4x.0628x.63x10^3	1,630
	1000 (unload)	A Compr.	[.45(23.3+15.0)/2+(.40x23.3/2)]2	26.6
		A Tension	8.8x2x2.03	35.7
		Moment	26.6x.60x.0628x10^3	1,000.
	1550	A Compr.	[30.0(.89+.62)/2]2	45.3
		A Tension	14.0x2x2.03	56.9
		Moment	45.3x.57x.0628x10^3	1,620

Figure 38: Check of Stress Distribution Curves by Area and Moment Balance

Figure 39

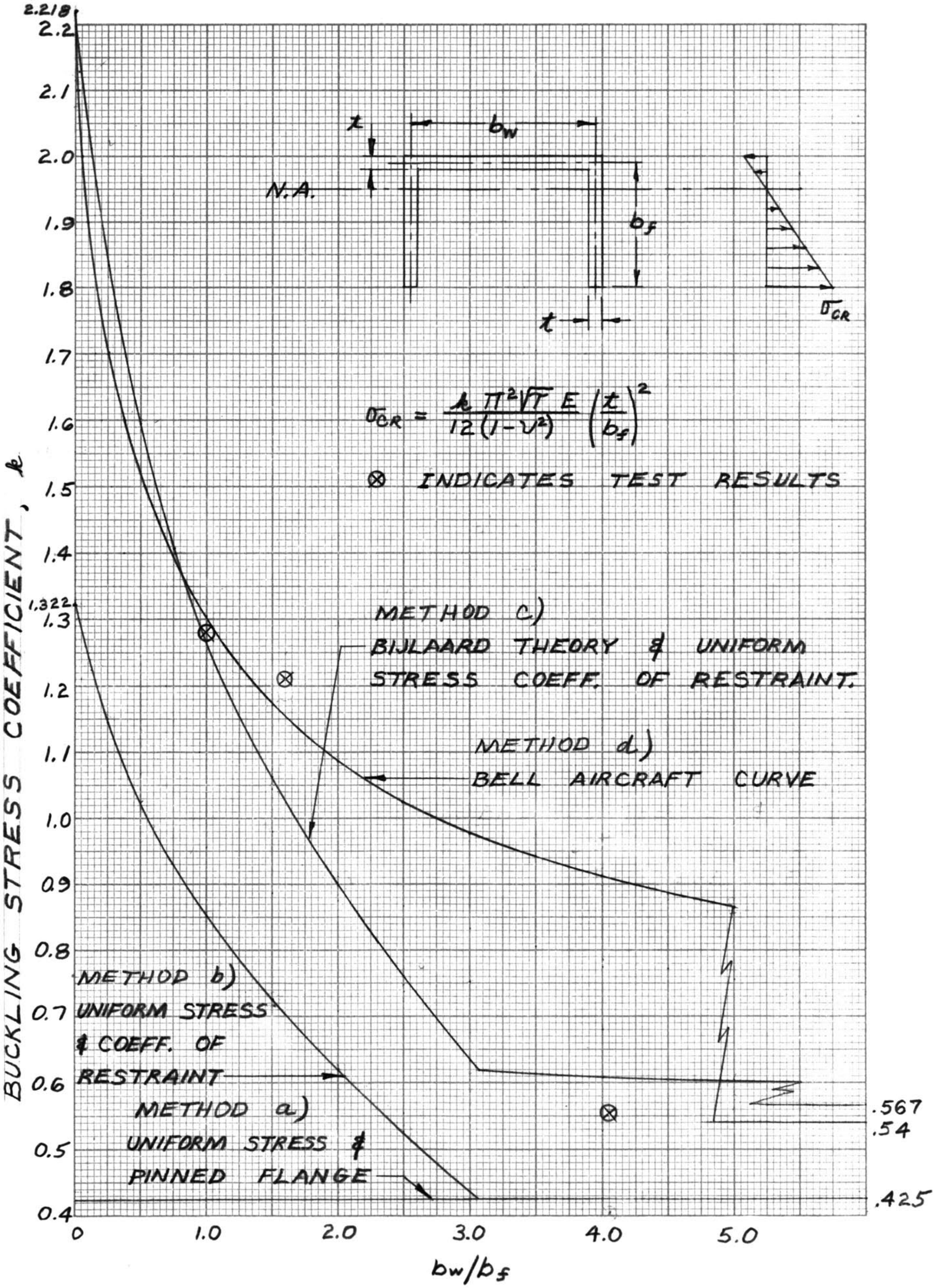
2.218
2.2
2.1
2.0
1.9
1.8
1.7
1.6
1.5
1.4
1.322
1.3
1.2
1.1
1.0
0.9
0.8
0.7
0.6
0.5
0.4
0
1.0
2.0
3.0
4.0
5.0
bw/bf
BUCKLING STRESS COEFFICIENT, k
t
b_W
N.A.
b_f
t
σ_{CR}
$\sigma_{CR} = \frac{k \pi^2 \sqrt{T} E}{12(1-\nu^2)} \left(\frac{t}{b_f}\right)^2$
⊗ INDICATES TEST RESULTS
METHOD c)
BIJLAARD THEORY & UNIFORM
STRESS COEFF. OF RESTRAINT.
METHOD d)
BELL AIRCRAFT CURVE
METHOD b)
UNIFORM STRESS
& COEFF. OF
RESTRAINT
METHOD a)
UNIFORM STRESS &
PINNED FLANGE
.567
.54
.425

1	2	3	4	5	6	7	8	9	10	11	12	13
b_w/b_f	$\frac{2+b_w/b_f}{1+b_w/b_f}$	$\frac{16.8}{\pi^2(4-\alpha)}$	$(k_B)_f$	$.106(\frac{b_w}{b_f})^2$	$\frac{b_w/b_f}{1-.106(\frac{b_w}{b_f})^2}$	3δ	$\frac{2}{3\delta+4}$	$\sqrt{k_r}$ $.65\frac{2}{3\delta+4}$	k_r	$\frac{k_r-.425}{.852}$	$(k_B)_f-(k_B)_h$	k_B $\frac{k_r-.425}{.852}[(k_B)_f-(k_B)_h]+(k_B)_h$
0	2.00	.850	2.15	0	0	0	.500	1.150	1.322	1.051	1.300	2.218
.0250	1.973	.839	2.13	0	.0250	.075	.491	1.141	1.302	.998	1.291	2.128
.125	1.889	.807	2.09	.00166	.1252	.3756	.457	1.107	1.225	.939	1.283	2.012
.250	1.800	.774	2.03	.00662	.252	.756	.420	1.070	1.144	.844	1.256	1.833
.500	1.667	.730	1.96	.0265	.514	1.542	.362	1.012	1.024	.703	1.230	1.595
.750	1.571	.703	1.89	.0596	.798	2.394	.314	.964	.929	.591	1.187	1.405
1.000	1.500	.680	1.86	.1060	1.119	3.36	.272	.922	.850	.499	1.180	1.269
1.500	1.400	.654	1.81	.238	1.970	5.91	.202	.852	.726	.353	1.156	1.062
2.000	1.333	.637	1.77	.424	3.47	10.41	.139	.789	.622	.231	1.133	.899
2.500	1.286	.627	1.75	.662	7.40	22.2	.076	.726	.527	.1199	1.123	.762
3.00	1.25	.619	1.73	.954	65.2	195.6	.010	.660	.435	.0117	1.111	.632
3.07	1.247	.619	1.73	1.00	∞	∞	0	.650	.425	0	-	.619
4.00	1.20	.608	1.65	-	∞	∞	0	.650	.425	0	-	.608
5.00	1.167	.601	1.69	-	∞	∞	0	.650	.425	0	-	.601
	1.000	.567	1.61	-	∞	∞	0	.650	.425	0	-	.567

Figure 41: Table Calculating k Values for Methods (b) and (c).

5.0 Discussion of Results

5.1 Critical Moment

The test results of critical stresses showed very good agreement with theoretical methods (a) and (b). They indicated that methods (c) and (d) were too conservative.

The large variations of k in the different theoretical methods did not appreciably effect the crippling stress in the inelastic range. However, in the elastic range the critical stress was directly proportional to k. For this reason for the materials used methods (a) and (b) predicted critical stresses which were almost identical. However, for a material with a proportional limit above 20 ksi, method (b) would predict conservative stresses when the ration of b_w/b_f was greater than 1.6.

Channel #2, which buckled at 19 ksi, seemed to indicate better agreement with method (a) than method (b). This was the area on figure 39 where curves (a) and (b) began to separate and indicated that method (a) gave better results in the high ratios of b_w/b_f. However, the results were not conclusive on this point.

5.2 Ultimate Moment

For each channel section an ultimate moment was recorded which was somewhat greater than the critical buckling moment. A semi-empirical method was developed for predicting this moment.

Assume at ultimate moment the web was completely in tension and the flange in compression. Assume the stress in the compression flange was equal to the extreme fibre buckling stress and the tension web was at some stress not greater than the material yield point.

Consider figure 45, if the flange stress was σ_{cr}, and since the tension area equalled the compression area, then, by proportioning, the web stress was approximately (for one flange)

$$\sigma_{cr} \frac{b_f t}{\frac{b_w}{2} t} = \frac{2 \sigma_{cr} b_f}{b_w} \quad . \quad (17)$$

For most practical channel dimensions and most materials it was found that the web stress was less than σ_y. Therefore, figure 45 seemed like a reasonable assumption for a first approximation of the stress distribution at ultimate moment.

Consider the stress distributions at ultimate load for the various channel (figures 35, 36 and 37). Channel #1, with a deep flange first buckled at a low extreme fibre stress. However, after buckling the extreme fibre still maintained the critical stress. As the moment kept increasing the stress in the fibres closer to the web increased to their critical stress, and the neutral axis shifted down. The fibres inside the extreme fibre all buckled at higher critical stresses than the extreme fibre, so the actual stress distribution looked like the 7,000 in-lb moment condition in figure 35. Finally the moment got so large that the flange buckled completely. The fibres immediately adjacent to the web took small stresses since the propagation of the buckle created local stresses which failed these fibres. The actual distribution in figure 35 may be approximated by the theoretical distribution in figure 45.

A similar stress distribution occurred in channel #3 where the critical stress was very close to the yield. In this case the critical stress occurred on down to the fibres quite close to the neutral axis, and failure was analogous to that of a cross section not critical in local crippling.

However, in the case of channel #2 where the critical extreme fibre stress was close to the proportional limit, the critical stress did not increase in the fibres closer to the web. The buckle propagation occurred earlier and the ultimate moment was only slightly greater than the critical moment. This stress distribution at ultimate is shown by the 4,750 in-lb moment condition in figure 36, and was close to a triangular distribution.

In consideration of these observations it was decided to predict ultimate moment by the distribution of figure 45, and reduce it by a factor to fit the cases of the individual channels. The ultimate moment by the distribution of figure 45 was:

$$M_{ult} = 2\,\sigma_{cr}\, b_f t\, \frac{b_f}{2} = \sigma_{cr}\, b_f^{\,2} t \tag{18}$$

where:

M_{ult} = ultimate moment

σ_{cr} = critical buckling stress at the extreme fibre calculated by method (a).

This moment was reduced by some function of the two ratios (σ_y/σ_{cr}) and (t/b_f). A factor that fitted the test results was

$$M_{ult} = \sigma_{cr}\, b_f^{\,2} t\, (\mathfrak{F}) \tag{19}$$

where:

$$\mathfrak{F} = 16.0 \left(\frac{\sigma_y}{\sigma_{cr}}\right) \left(\frac{t}{b_f}\right)$$

Equation (19) had as its lower limit the case of a triangular stress distribution and as its upper limit a rectangular stress distribution. Therefore equation (19) was written as follows:

$$M_{ult} = .667\,\sigma_{cr}\, b_f^{\,2} t \qquad \text{where } 16.0\,\frac{\sigma_y}{\sigma_{cr}}\,\frac{t}{b_f} < .667 \tag{19a}$$

$$M_{ult} = \sigma_y\, b_f t^2 (\mathfrak{F}) \qquad \text{where } 1.0 > 16.0\,\frac{\sigma_y}{\sigma_{cr}}\,\frac{t}{b_f} > .667 \tag{19b}$$

$$M_{ult} = \sigma_{cr}\, b_f^{\,2}\, t \qquad \text{where } 16.0\,\frac{\sigma_y}{\sigma_{cr}}\,\frac{t}{b_f} > 1.0 \tag{19c}$$

Applying these equations to the channels tested and comparing to the ultimate moments gave the results of figure 40. Positive error indicated the test results were higher.

Channel	Test Results M_{ult}(in.-lbs.)	M_{ult}, Eqns. (19c)&(19d)	%Error
#1	7,250	7,100	+ 2.1
#2	4,750	4,600	+ 3.2
#3	1,550	1,735	-11.9

Figure 40: Table of Percent Error Between Actual Ultimate Moment and Predicted Ultimate Moment

6.0 Conclusions

As a result of studying test results, the following conclusions were reached.

6.1 Critical Moment

It was found that methods (a) and (b) of predicting buckling stresses showed good agreement with test results. Methods (c) and (d) were too conservative, especially in the region below the proportional limit.

Method (a)seemed to indicate better agreement than method (b), but more testing with different materials and different size channels was necessary to be sure.

From the discussion of paragraph 5.1, it was recommended to use method (a) for materials with a proportional limit below 18.0 ksi, and method (b) for other materials. This would assure a conservative design.

6.2 Ultimate Moment

From the discussion of paragraph 5.2 a semi-empirical approach of predicting ultimate moment was developed. Formulas that fit the test results were:

$$M_{ult} = .667\,\sigma_{cr}\,b_f^{\,2}t \qquad \text{where } 16.0\,\frac{\sigma_y}{\sigma_{cr}}\,\frac{t}{b_f} < .667 \tag{19a}$$

$$M_{ult} = \sigma_y b_f t^2(\mathcal{F}) \qquad \text{where } 1.0 > 16.0\,\frac{\sigma_y}{\sigma_{cr}}\,\frac{t}{b_f} > .667 \tag{19b}$$

$$M_{ult} = \sigma_{cr} b_f^{\,2} t \qquad \text{where } 16.0\,\frac{\sigma_y}{\sigma_{cr}}\,\frac{t}{b_f} > 1.0 \tag{19c}$$

where σ_{cr} was the extreme fibre crippling stress as given by method (a) and $\mathcal{F} = 16.0\,\frac{\sigma_y}{\sigma_{cr}}\,\frac{t}{b_f}$

More testing was necessary to substantiate these results. A temporary method of predicting ultimate moment which gave conservative results for all cases was given by equation (19a).

7.0 References

1. "Bell Aircraft Corporation Structures Manual", 1955.
2. Bijlaard, P.P.; "Buckling of Plates Under Non-homogeneous Stress", ASCE Proceedings, 1957 1293 EM3.
3. Bleich, Friedrich; "Buckling Strength of Metal Structures", McGraw-Hill Book Co., 1952.
4. Lundquist, E.E., Stowell, E.A., and Schuette, E.H.; "Principles of Moment Distribution Applied to Stability of Structures Composed of Bars and Plates". NACA ARR 3K06, November, 1943.
5. Lundquist, E.E. and Stowell, E.A.; "Critical Compressive Stress for Outstanding Flanges", NACA TR 734, 1942.
6. Timoshenko, Stephen; "Theory of Plates and Shells", McGraw-Hill Book Co., 1940.
7. Timoshenko, Stephen; "Theory of Elastic Stability", McGraw-Hill Book Co., 1936.
8. Stowell, E.A.; "A Unified Theory of Plastic Buckling of Columns and Plates", NACA Technical Note 1556, 1948.
9. Gerard, George; "The Crippling Strength of Compression Elements", Journal of the Aeronautical Sciences, January, 1958.
10. "ASTM Standards", Tensile Test Procedure E8-54T.

8.0 Appendices

The following illustrations were included in the appendices.

1. Photos of test apparatus. (figures 1 through 6)
2. Sketch of channel testing apparatus. (figure 7)
3. Sketch of tensile specimen. (figure 8)
4. Sketch of channel section. (figure 9)
5. Stress distribution factor, . (figure 42)
6. Stress distribution in channel section. (figure 43)
7. Analysis of flange by method (d). (figure 44)
8. Theoretical ultimate moment stress distribution. (figure 45)

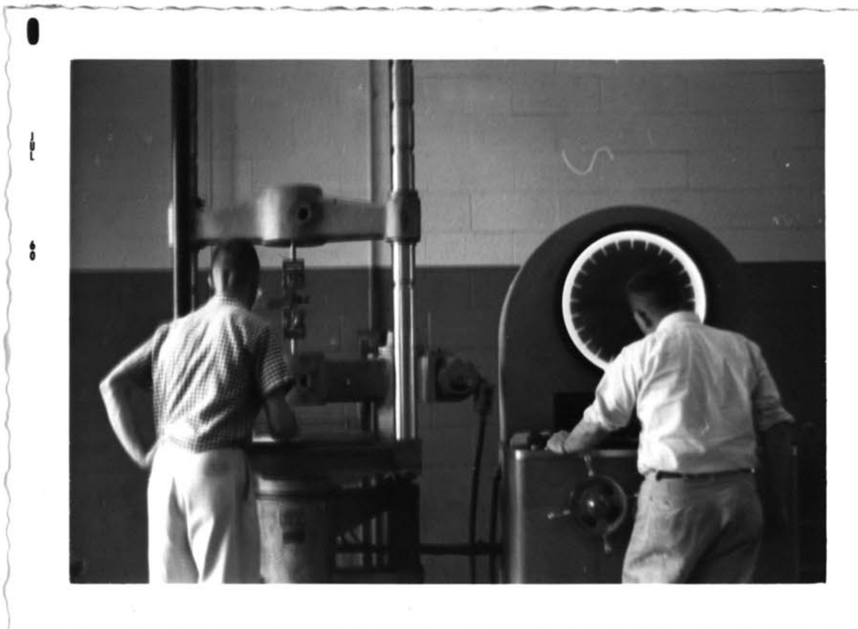

Figure 1: Photo - Tensile Testing Apparatus

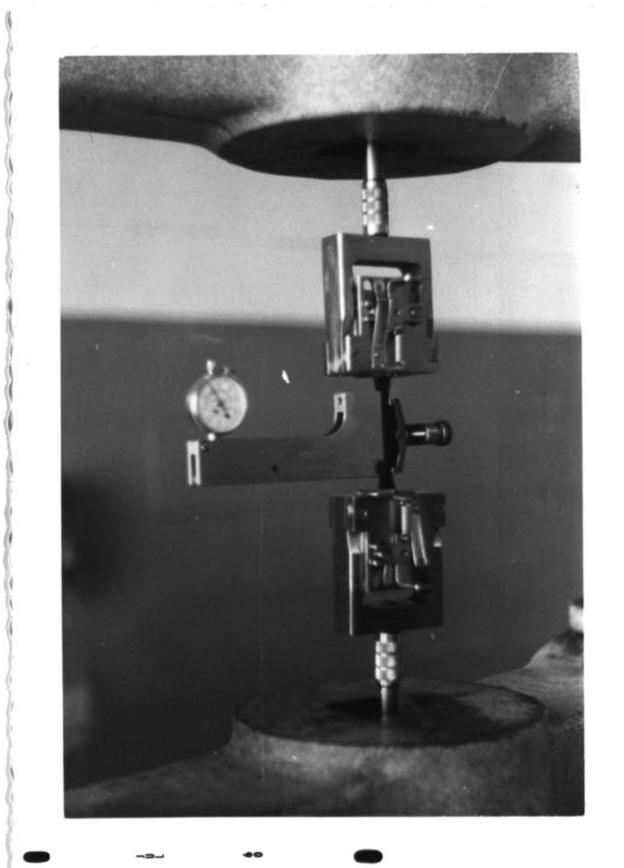

Figure 2: Photo - Tensile Testing Specimen in Machine

Figure 3: Photo - Channel Test Sections Showing Strain Gages

Figure 4: Photo - Channel Section in Testing Machine

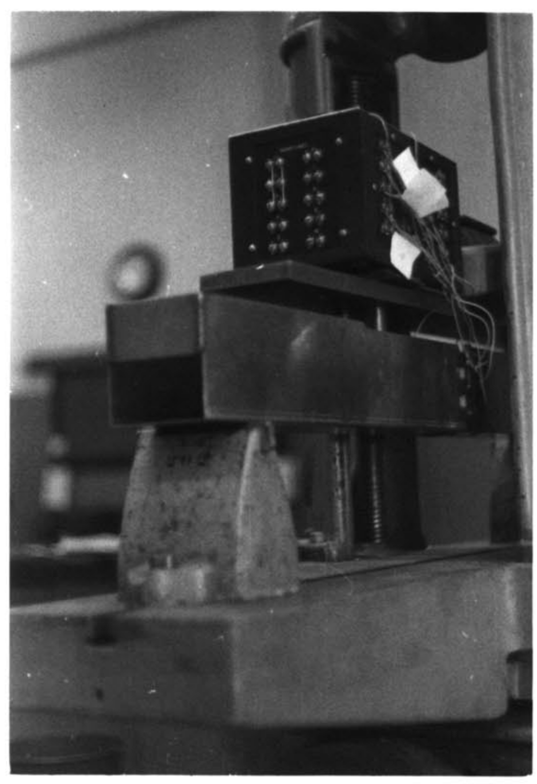

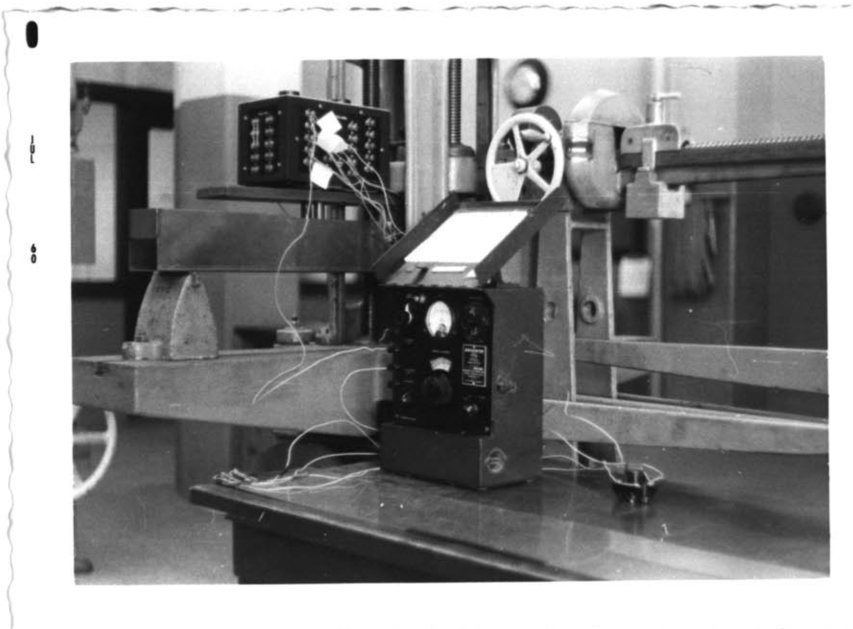

Figure 5: Photo - Channel Section and Strain Indicator

Figure 6: Photo - Balancing Strain Indicator

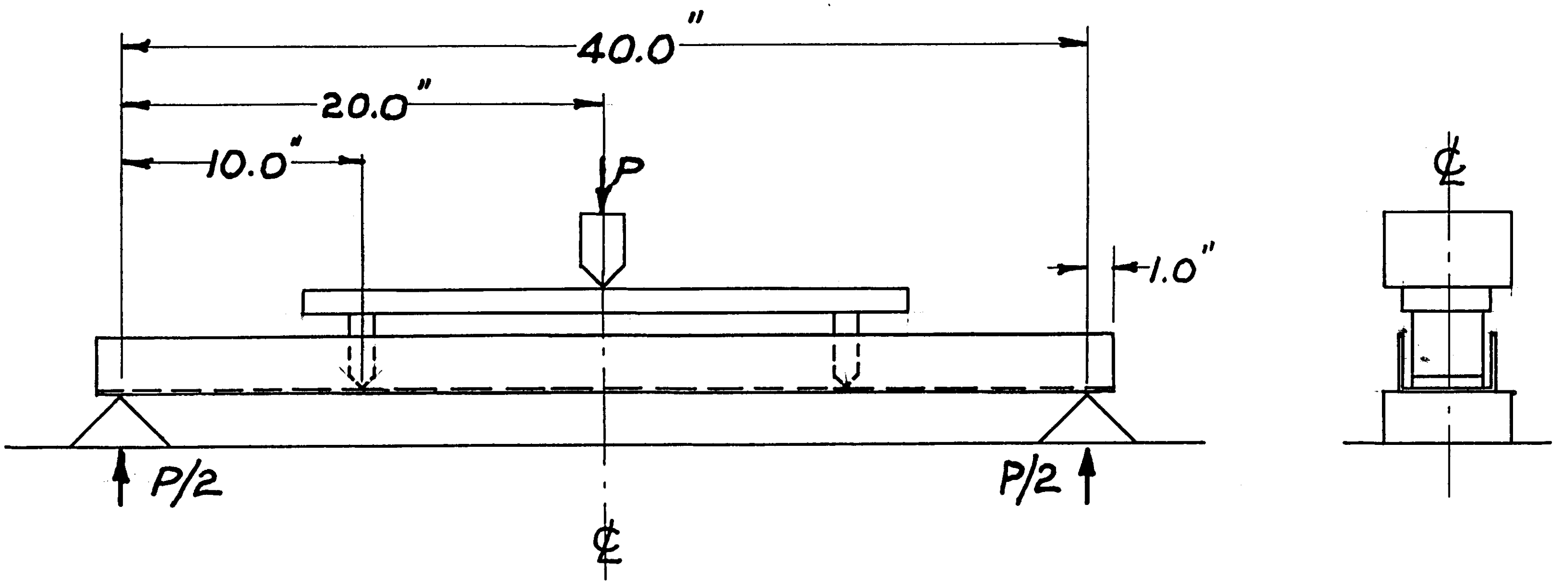

CHANNEL TESTING APPARATUS

Figure 7

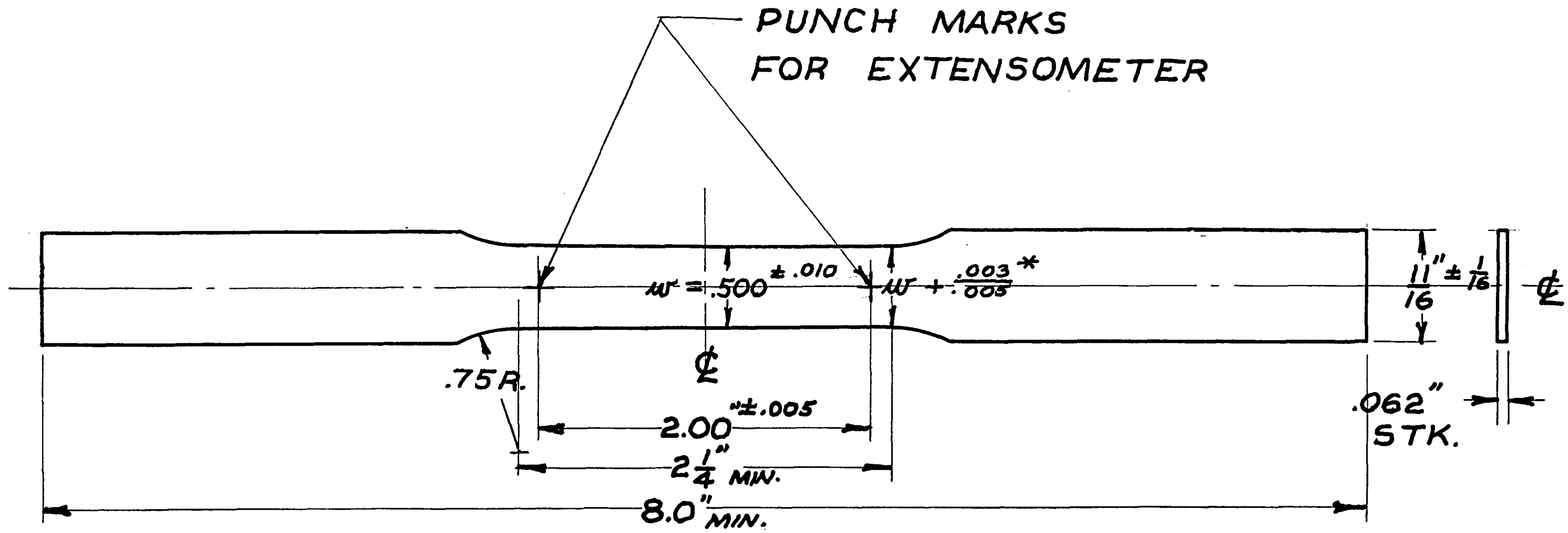

*GRADUAL TAPER FROM ℄ TEST SECTION TO END.

TENSILE SPECIMEN

Figure 8

SECTION	a ±.020
#1	4.00
#2	2.50
#3	1.00

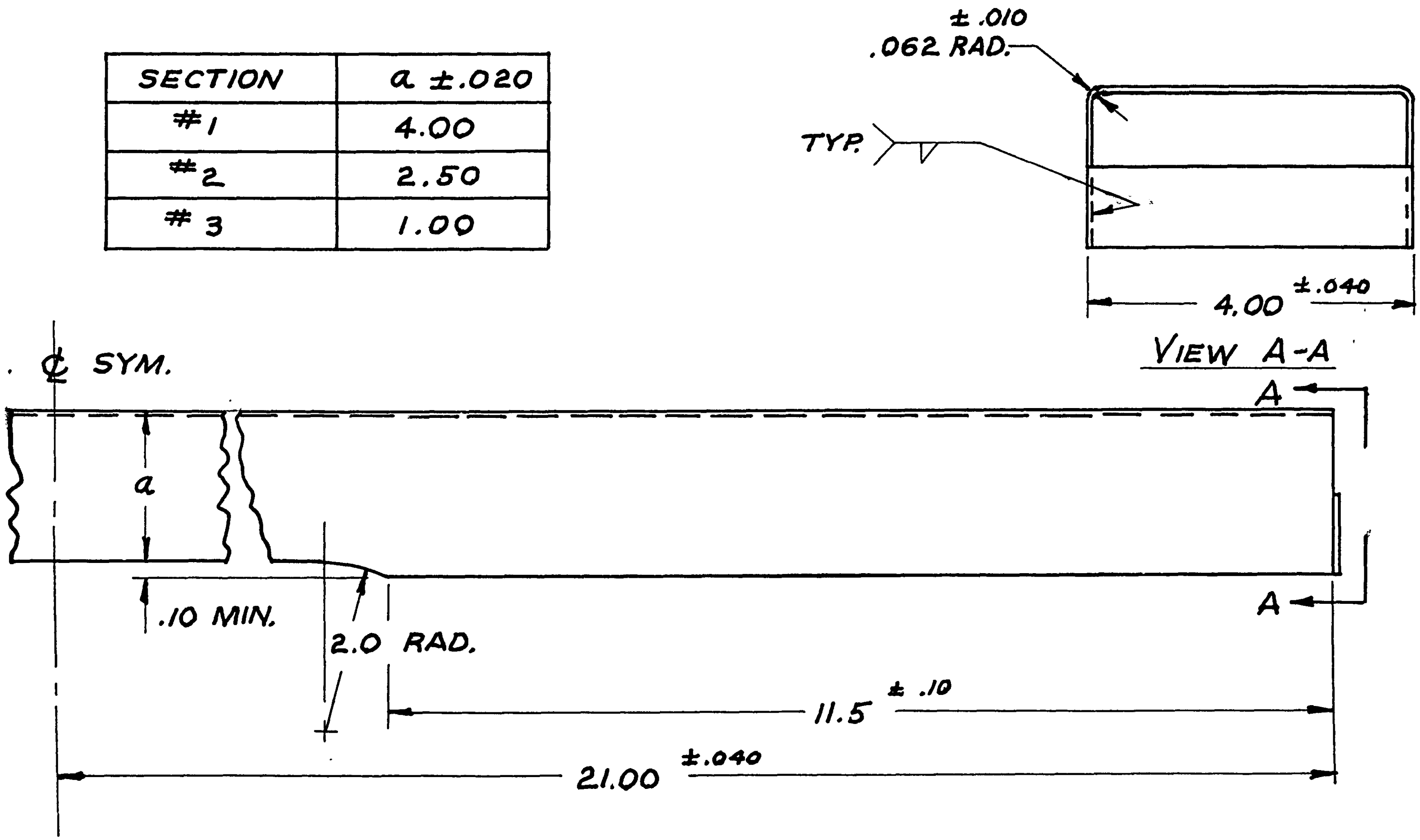

MATL. - .062 C.R. ANNEALED STOCK

GRIND FREE OF ALL BURRS

DO NOT POUND INTO SHAPE

CHANNEL SECTION

Figure 9

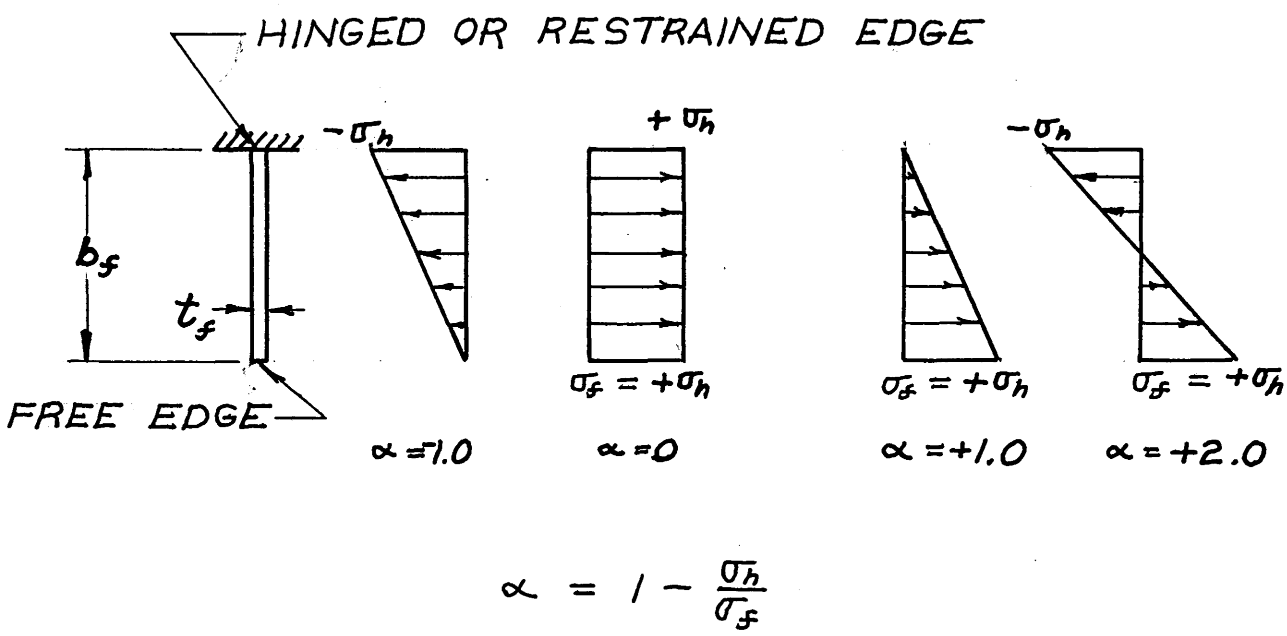

Figure 42: Illustration of Stress Distribution Factor, α

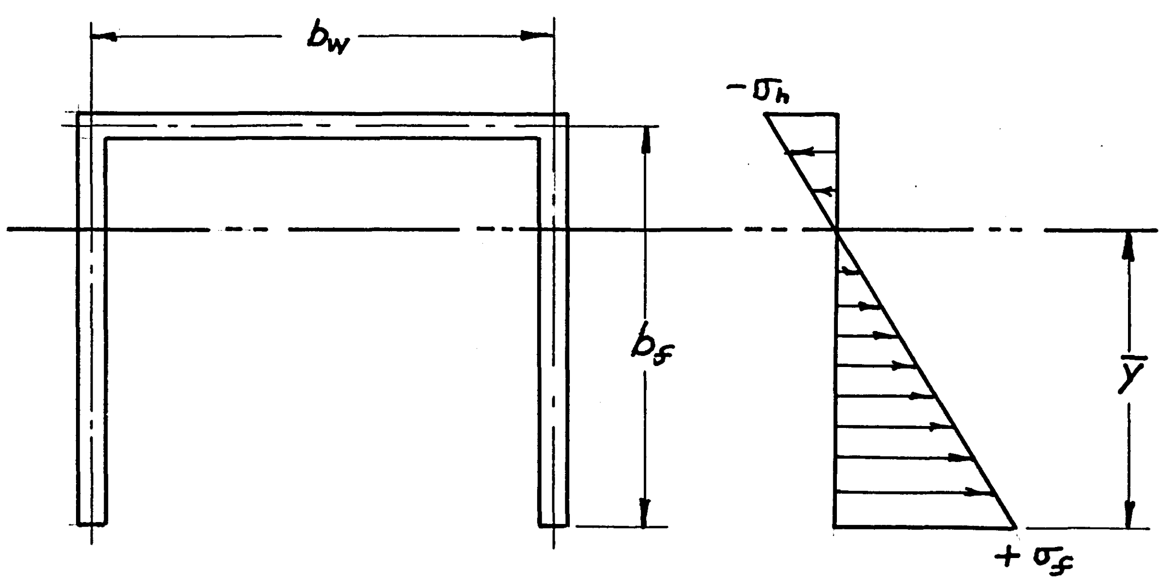

Figure 43: Illustration of Stress Distribution in Channel Section

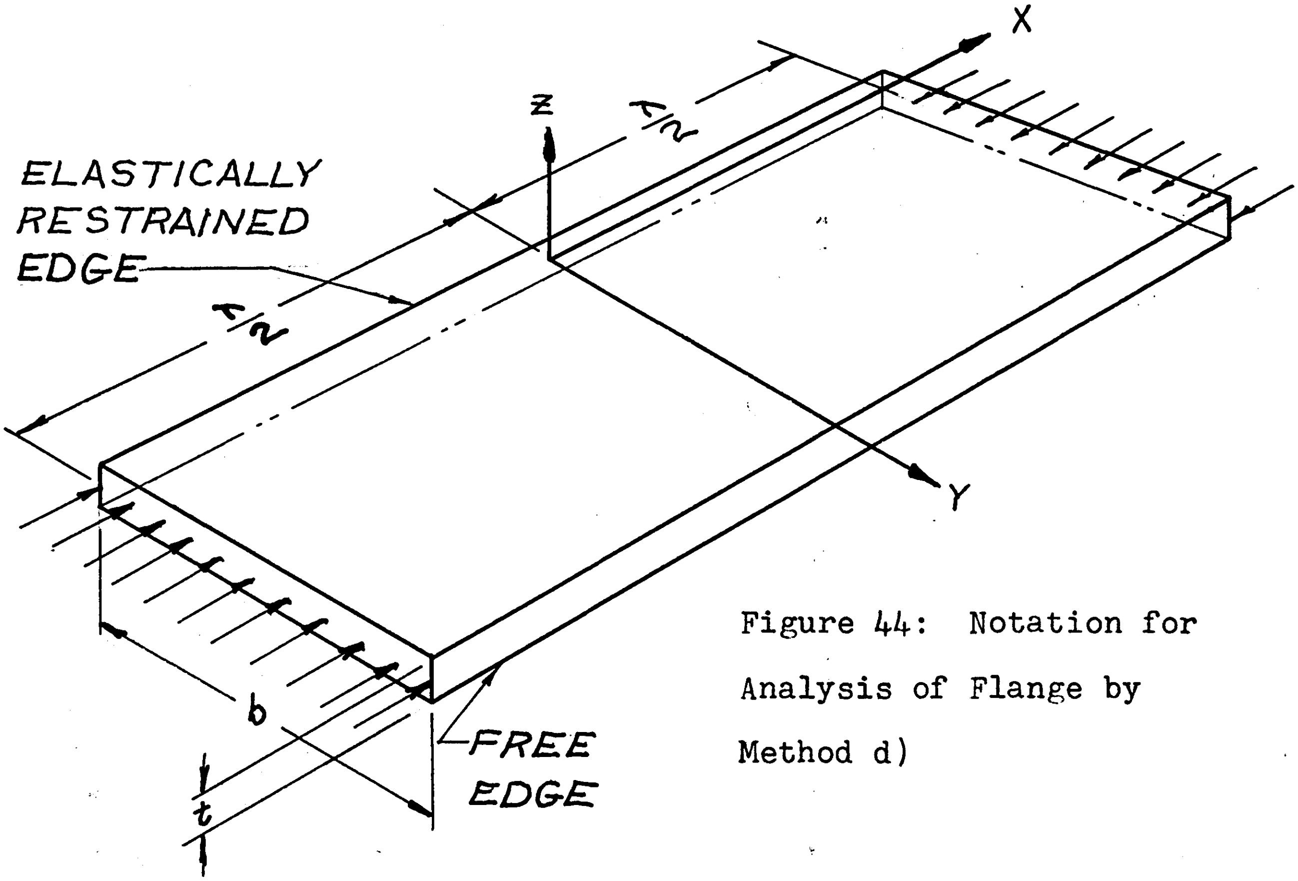

Figure 44: Notation for Analysis of Flange by Method d)

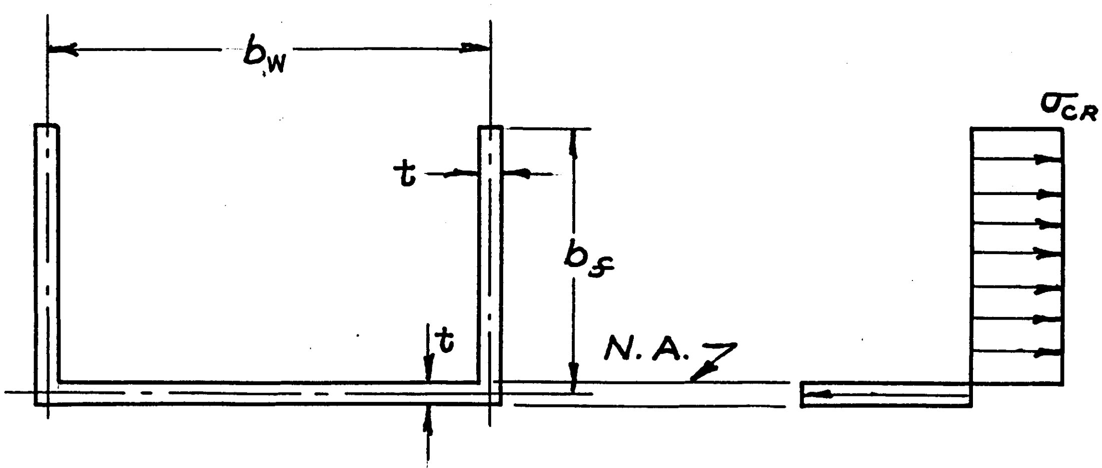

Figure 45: Theoretical Ultimate Moment Stress Distribution